RSC Advances

REVIEW

View Article Online
View Journal | View Issue

Cite this: *RSC Adv.*, 2026, **16**, 21487

Recent advances in functional materials for uranium monitoring through optical and electrochemical techniques

KaiZeng Quan,†[a] YuMin Wang,†[b] Meng Qi,[a] Peng Xu,[a] YaXing Wang[b] and GuoXun Ji*[a]

Received 17th March 2026
Accepted 9th April 2026

DOI: 10.1039/d6ra02232d

rsc.li/rsc-advances

Uranium is a naturally occurring element widely employed in nuclear energy production and various industrial applications. However, it poses substantial risks to the environment and human health due to its combined radiological and chemical toxicity, thereby making rapid, accurate, and field-deployable detection technologies critical. Conventional detection methods, including atomic absorption or fluorescence spectroscopy and inductively coupled plasma spectroscopy, are limited by their high costs, complicated operational procedures, and dependence on specialized laboratory facilities, which severely restrict their practical on-site applications. To address these limitations, significant advances have been made in recent years in the development of functional materials for uranium sensing, especially metal–organic frameworks (MOFs), covalent organic frameworks (COFs), nanomaterials, DNAzymes, and other emerging materials. These materials support versatile optical and electrochemical detection strategies, such as fluorescence, colorimetry, and electrochemical sensing, which offer high sensitivity, fast response, and considerable potential for real-time field monitoring. This review highlights recent advances in the detection mechanisms, sensing performance, and practical advantages and limitations of various sensing systems. Finally, a comparative analysis is presented to identify key challenges and provide perspectives for the future development of efficient and reliable uranium detection technologies.

1. Introduction

Uranium, a naturally occurring radioactive element, plays a critical role in both the energy and defense sectors as a primary nuclear fuel.[1–3] As a high-energy-density energy source, uranium is indispensable for nuclear power generation, whereas its involvement in nuclear weapons testing, atomic bombings, and the deployment of depleted uranium munitions has led to extensive nuclear pollution. Major nuclear accidents, including those at Chernobyl and Fukushima, have further exacerbated environmental contamination.[4–6] The radiological and chemical toxicity of uranium presents considerable risks to ecological systems and human health. In aqueous environments, uranium mainly exists in the form of the uranyl ion (UO_2^{2+}), and its excessive accumulation results in persistent environmental contamination. Radiation emitted during uranium decay can cause cellular damage and elevate cancer risks, while its chemical toxicity exerts adverse effects on vital organs, including the kidneys, liver, and bones.[7–9] The World Health Organization has established a maximum contaminant limit of 30 μg L^{-1} for uranium in drinking water, underscoring the urgent demand for effective monitoring techniques. Accordingly, the development of rapid, highly selective detection materials for UO_2^{2+} in aqueous systems has emerged as a major research direction.[10,11]

Traditional methods for detecting UO_2^{2+} in aqueous solutions, including atomic absorption spectroscopy,[12] atomic fluorescence spectroscopy,[13] and inductively coupled plasma spectroscopy,[14] are limited in their widespread application by high costs and complex operational requirements.[15] In contrast, newer techniques such as fluorescence, colorimetry, and electrochemical detection provide more practical alternatives.[16–19] Fluorescence methods are particularly recognized for their high sensitivity and rapid response,[20] while colorimetric detection is valued for its simplicity and visual readout capability.[21] Electrochemical detection, characterized by its low detection limits, is especially well-suited for complex environmental samples.[22] In recent years, advanced materials, including metal–organic frameworks (MOFs), covalent organic frameworks (COFs), nanomaterials, and DNAzymes, have attracted significant attention for their potential in uranium detection.[23–26] MOFs and COFs stand out due to their porous

[a]*Rocket Force University of Engineering, Xi'an 710025, PR China. E-mail: ji_guoxun@sina.com*

[b]*State Key Laboratory of Radiation Medicine and Protection, School for Radiological and Interdisciplinary Sciences (RAD-X) and Collaborative Innovation Center of Radiation Medicine of Jiangsu Higher Education Institutions, Soochow University, Suzhou 215123, PR China*

† These authors contributed equally.

structures, high specific surface areas, and tunable functional groups, which make them ideal candidates for UO_2^{2+} detection.[27,28] Nanomaterials, with their excellent optical and electrical properties, can be surface-functionalized to achieve the selective detection of UO_2^{2+}.[25] DNAzymes, which leverage the biomolecular recognition capabilities of DNA, further enhance the selectivity of UO_2^{2+} detection.[29] These functional materials offer substantial advantages, rendering them highly promising for the future development of uranium detection technologies.

Over the past few years, several reviews focusing on UO_2^{2+} detection have been published. Specifically, in 2022, Liu *et al.*[30] reviewed the advances in the adsorption, detection, and synchronous application of MOF-based materials for U(VI) in aqueous solutions. In 2023, Rani *et al.*[31] summarized the research progress of various nanomaterials (*e.g.*, metal nanoparticles and carbon-based materials) in uranium detection and removal. In 2024, Sharma *et al.*[32] analyzed the advantages and limitations of electrochemical techniques based on chemically modified electrodes for the detection of radionuclides, such as uranium and cesium. In 2025, Sun *et al.*[33] elaborated on the preparation and characterization of carbon dots and their composites, along with their applications, mechanisms, and challenges in the detection and adsorption of uranium and other radioactive elements. In the same year, Poulin-Ponnelle *et al.*[34] reviewed the research progress on fluorescent probes for toxic elements associated with the nuclear industry (*e.g.*, uranium and cesium), covering multiple sensing platforms, fluorescence mechanisms, and application prospects. However, most of these reviews tend to focus on specific material categories or individual detection methods rather than providing a comprehensive overview. In view of this, the present review summarizes the recent progress in UO_2^{2+} detection by covering a wide spectrum of representative sensing materials, including MOFs,[35] COFs,[36] nanomaterials,[31] DNAzymes,[37] and other functional systems. Notably, this work provides the first comprehensive cross-material and cross-technique comparative analysis of UO_2^{2+} sensing platforms. We systematically examine the sensing mechanisms, analytical performance, and structure–property relationships of various material systems, critically evaluate their respective advantages and limitations, and further discuss key challenges that hinder their practical deployment, as well as feasible pathways for future improvement. Through this integrated and forward-looking perspective, the review aims to deliver a holistic understanding of UO_2^{2+} detection and provide valuable guidance for the rational design of next-generation high-performance uranium sensing platforms.

2. Fluorescence

Fluorescence is an analytical technique based on photoluminescence, with its mechanism varying depending on the type of material used.[38] By tailoring the chemical structures or surface properties of fluorescent probes, these probes can be engineered to interact specifically with a target analyte, thereby inducing a distinct change in fluorescence. This allows for the detection of the target substance through the monitoring of corresponding signal variations (Fig. 1).[39]

2.1 MOFs

MOFs are a new class of porous materials that have emerged rapidly over the past few decades. They are constructed from metal ions or clusters connected to organic ligands through coordination bonds, forming crystalline structures with periodic networks, high porosity, and large specific surface areas.[40] Due to these distinctive properties, MOFs have been widely applied in numerous fields, among which the design of fluorescent sensors based on their fluorescent characteristics has become a prominent research focus.[41]

2.1.1 Fluorescence mechanism of MOFs. The luminescence derived from the metal centers in MOFs is predominantly associated with lanthanide ions, such as Eu^{3+} and Tb^{3+}. This luminescence originates from 4f–4f electronic transitions; since these transitions are Laporte-forbidden, the direct excitation of the lanthanide ions is inefficient.[42] To address this limitation, organic ligands function as antennas: they absorb incident light

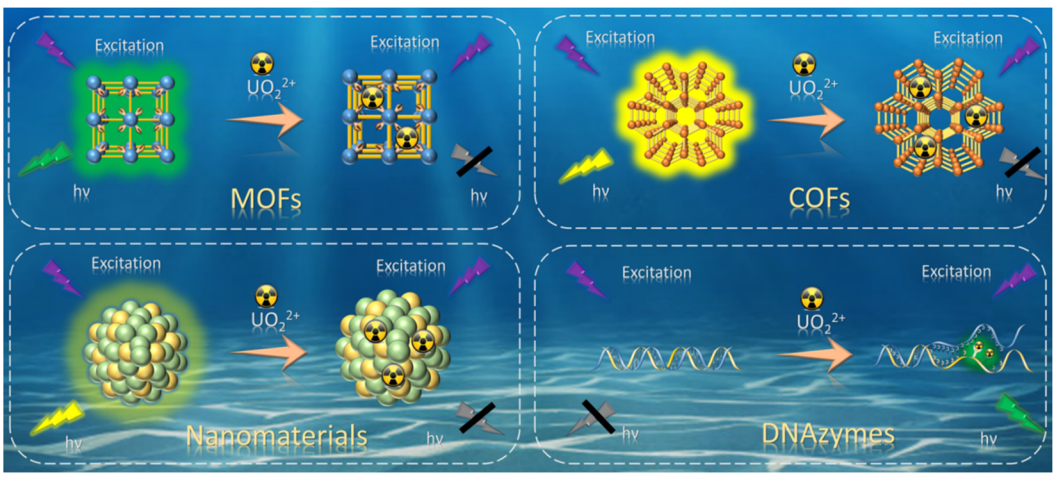

Fig. 1 Schematic of the fluorescence detection of UO_2^{2+} with different materials.

and subsequently transfer the absorbed energy intramolecularly to the metal center. This process, commonly referred to as the "antenna effect", promotes the lanthanide ion to an excited state. The ion then returns to its ground state through radiative decay, emitting its characteristic sharp-line fluorescence. This efficient sensitization strategy renders lanthanide ions ideal emissive centers in luminescent MOFs.[43]

In addition to metal-centered luminescence, luminescence from ligand centers primarily arises from $\pi \rightarrow \pi^*$ or $n \rightarrow \pi^*$ electronic transitions within the π-conjugated system of the organic ligands.[44] The rigid crystalline framework of MOFs significantly suppresses non-radiative relaxation processes, such as molecular vibrations and rotations of the ligands, through spatial confinement effects, thereby substantially enhancing the fluorescence quantum yield. In certain systems, additional mechanisms, such as intermolecular charge transfer (CT) or aggregation-induced emission (AIE), are also involved. Furthermore, by tuning the energy-level alignment, electronic properties, and geometric structure between the metal and organic ligands, a variety of luminescence mechanisms can be achieved, including ligand-to-ligand charge transfer, metal-to-metal charge transfer, and metal-to-ligand or ligand-to-metal charge transfer.[45]

2.1.2 Fluorescent MOFs for UO_2^{2+} detection. UO_2^{2+} exhibits a linear geometry and possesses multiple vacant coordination sites in its equatorial plane, enabling it to coordinate with oxygen or nitrogen donor atoms from the carboxyl or amino groups of MOF organic linkers.[46] This coordination interaction induces changes in the fluorescence intensity of the MOF, and UO_2^{2+} detection is therefore achieved by monitoring such fluorescence variations, including fluorescence quenching, enhancement, or ratiometric fluorescence signals.[47]

Fluorescence quenching primarily operates through three mechanisms: photoinduced electron transfer (PET), fluorescence resonance energy transfer (FRET), and the inner filter effect (IFE).[48] In PET, excited-state electrons from the fluorescent MOF are transferred to UO_2^{2+}, creating a non-radiative relaxation pathway back to the ground state and resulting in significant fluorescence reduction.[49] FRET occurs when the emission spectrum of the MOF overlaps considerably with the absorption spectrum of UO_2^{2+}, allowing non-radiative energy transfer to UO_2^{2+} and subsequent fluorescence quenching.[50] IFE arises when the fluorescent material itself or other light-absorbing species absorb either the excitation or emitted light, leading to decreased fluorescence intensity.[51] Qin *et al.*[52] synthesized a Zn-based MOF (HNU-50), whose fluorescence originates from the π-conjugated system of the pyromellitic acid (PMA) ligand. The uncoordinated oxygen atoms on the ligand serve as binding sites for UO_2^{2+} (Fig. 2A). A notable spectral overlap was observed between the emission spectrum of the PMA ligand and the absorption spectrum of uranyl nitrate in the 335–476 nm region. Consequently, UO_2^{2+} absorbs the emission from the PMA ligand, leading to fluorescence quenching of HNU-50 *via* the FRET mechanism.

In contrast to fluorescence quenching, fluorescence enhancement is primarily achieved through two distinct mechanisms: inhibition of non-radiative energy transfer and

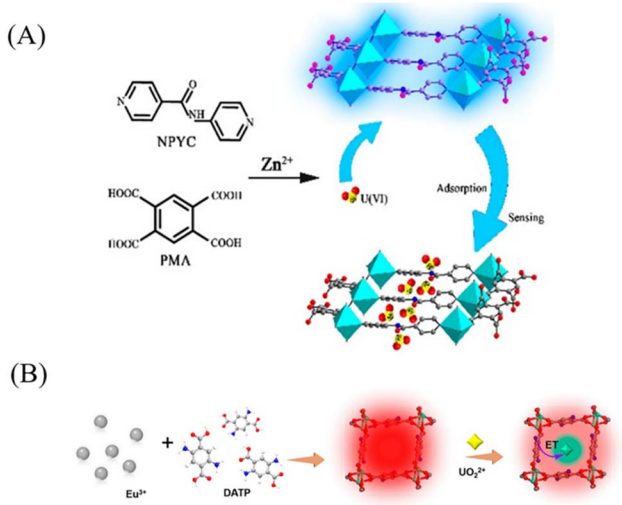

Fig. 2 (A) Mechanism of HNU-50 fluorescence detection of uranyl ions. Reproduced with permission from ref. 52. Copyright 2020, the American Chemical Society. (B) Schematic of the preparation of Eu-DATP and its application for UO_2^{2+} analysis. Reproduced with permission from ref. 55. Copyright 2024, the American Chemical Society.

sensitization of the intrinsic luminescence of uranyl ions. For MOFs with lanthanide-centered emission, coordination of UO_2^{2+} to the MOF can induce structural rigidification, which significantly reduces non-radiative energy loss and enhances the efficiency of the "antenna effect", thereby markedly boosting the characteristic fluorescence of the lanthanide ions. Alternatively, when UO_2^{2+} coordinates with the organic ligands in the MOF, energy transfer from the ligands to the uranyl ion may occur, which sensitizes and activates the intrinsic emission of UO_2^{2+} itself. Both of these mechanisms can be effectively utilized to construct fluorescence-enhanced sensors for UO_2^{2+} detection.

Ratiometric sensing for UO_2^{2+} detection utilizes the ratio of emission intensities at two distinct wavelengths from a fluorescent probe as the response signal.[53] This relative signal change enables the sensitive and accurate quantification of UO_2^{2+}. Although UO_2^{2+} exhibits weak intrinsic photoluminescence, its coordination with organic ligands can significantly enhance its green emission at 509 nm *via* the "antenna effect", wherein the ligand transfers energy to UO_2^{2+}. Concurrently, this coordination process may alter the fluorescence emitted from the metal nodes or dopants within the MOF. By monitoring changes in the ratio of these dual emission signals, ratiometric sensing achieves highly precise and sensitive UO_2^{2+} detection.[54] For example, Tong *et al.*[55] developed a Eu-MOF with pore environments capable of simultaneously activating the intrinsic fluorescence of UO_2^{2+} and quenching the emission of Eu^{3+}, thereby constructing a dual-signal, inversely varying ratiometric fluorescent sensor (Fig. 2B). In this system, the organic ligand 2,5-diaminoterephthalic acid (DATP) absorbs light and transfers energy to Eu^{3+} *via* the antenna effect, resulting in its characteristic strong red emission. When UO_2^{2+} is captured and immobilized by the free amino groups within

the MOF channels, the energy absorbed by DATP is distributed to both Eu^{3+} and UO_2^{2+}. This leads to reduced energy transfer to Eu^{3+}, which attenuates its red emission, while the enhanced energy transfer to UO_2^{2+} intensifies its intrinsic green fluorescence. By calculating the intensity ratio at these two emission wavelengths, a concentration-dependent signal for UO_2^{2+} is established. This built-in self-referencing mechanism renders the ratiometric approach more reliable and resistant to interference than single-intensity-based detection.

2.2 COFs

Similar to MOFs, COFs are crystalline materials composed of light elements connected by covalent bonds, forming two- or three-dimensional topologies.[56] They are primarily constructed from aromatic organic ligands, such as phenyl, furan, and bipyridine units, which form extended covalent networks. Compared with MOFs, COFs are composed entirely of nonmetallic light elements, which endow them with superior thermal and chemical stability.[57] Additionally, COFs possess high specific surface areas, porous structures, strong fluorescence, and tunable chemical functionalities, making them versatile materials for a wide range of applications.[58]

2.2.1 Fluorescence mechanism of COFs. The fluorescence of COFs primarily originates from the photophysical properties of their organic building blocks and the unique effects induced upon framework formation. The emission mechanisms can be categorized into three main types: (1) intrinsic fluorescence of the building units. Most fluorescent COFs contain large π-conjugated aromatic moieties, such as pyrrole, bipyridine, triphenylbenzene, and carbazole, which exhibit strong fluorescence due to high $S_0 \rightarrow S_1$ transition probabilities and efficient $\pi^* \rightarrow \pi$ radiative relaxation. (2) Framework-induced fluorescence enhancement and modulation. The rigid covalent backbone restricts intramolecular rotations and vibrations, thereby suppressing non-radiative decay pathways and substantially enhancing emission intensity. Moreover, the close and ordered packing of emissive units within the framework can further modulate excited-state lifetimes and emission wavelengths. (3) Aggregation-induced emission effect. The incorporation of AIE-active units (*e.g.*, acridone or tetraphenylethylene) results in fluorescence quenching in isolated molecules due to intramolecular rotations; in contrast, confinement within the COF structure restricts these motions, leading to strong fluorescence upon aggregation.[59]

2.2.2 Fluorescent COFs for UO_2^{2+} detection. Fluorescent COFs designed with specific functional groups, such as hydroxyl, carboxyl, imine, and pyridine, can coordinate with UO_2^{2+} ions through coordination bonds.[60] Upon binding, UO_2^{2+} alters the local electronic environment, triggering photoinduced electron or energy transfer that results in fluorescence quenching.[61] Cui *et al.*[62] developed an sp^2-carbon-conjugated fluorescent COF (TFPT-BTAN-AO) containing triazine and cyano groups with excellent π-conjugation, which enables efficient light absorption and emission. The coordination of UO_2^{2+} with the amidoxime groups of the COF facilitates electron transfer from the COF to UO_2^{2+}, leading to significant fluorescence quenching with a detection limit of 6.7 nM (Fig. 3). Similarly, Zhen *et al.*[63] synthesized a novel olefin-linked COF (GC-TFPB-AO), featuring a π-conjugated system that produces stable fluorescence. UO_2^{2+} coordinates with the amidoxime, pyridine, and hydroxyl groups in the COF, inducing electron transfer from the organic ligands to UO_2^{2+} and effectively quenching the COF's fluorescence.

2.3 Nanomaterials

In addition to MOFs and COFs, nanomaterials have emerged as promising candidates for the detection and remediation of radioactive waste, owing to their unique physicochemical properties, including an exceptionally high surface area, ultrasmall size, quantum effects, and intrinsic fluorescence.[64] In recent years, their application in fluorescence-based detection of UO_2^{2+} has grown significantly, with metal nanoclusters and quantum dots as the primary examples.

2.3.1 Fluorescence mechanism of nanomaterials. Metal nanoclusters are nanoscale aggregates composed of several to hundreds of metal atoms (*e.g.*, gold, silver, or copper) and typically have a size of less than 2 nm.[65] They occupy a transitional state between discrete molecules and bulk solids. Owing to quantum confinement effects, nanoclusters exhibit discrete electronic energy levels, which allow electrons to undergo radiative transitions between these levels and return to the ground state.[66]

Another key type of nanomaterial for fluorescence-based UO_2^{2+} detection is quantum dots (QDs), which are

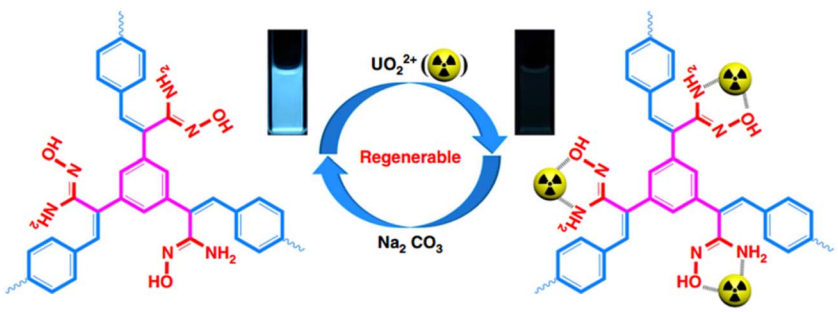

Fig. 3 Schematic of TFPT-BTAN-AO regeneration detection and extraction of UO_2^{2+}. Reproduced with permission from ref. 62. Copyright 2020, Springer.

semiconductor nanocrystals typically ranging in size from 2 to 10 nm. Their ultrasmall dimensions confine electrons and holes within the nanoscale domain, giving rise to quantum confinement effects that generate discrete and tunable electronic energy levels. Fluorescence emission from QDs arises from radiative transitions between these quantized energy states.[67]

2.3.2 Fluorescent nanomaterials for UO_2^{2+} detection. Gold nanoparticles (AuNPs) typically exhibit weak fluorescence and are mainly characterized by their surface plasmon resonance (SPR) absorption bands.[68] By leveraging the complementary spectral overlap between the absorption spectrum of AuNPs and the emission spectrum of gold nanoclusters (AuNCs), ratiometric fluorescence sensors based on the inner filter effect can be developed. For instance, Nan *et al.*[69] employed blue-emitting carbon dots (B-CDs) as an internal reference, whose fluorescence remains unaffected by changes in the UO_2^{2+} concentration. Upon interaction with UO_2^{2+}, the uranyl ion coordinates with the P═O and P–O groups on the AuNP surface, triggering the aggregation of AuNPs. This aggregation event causes a redshift and the broadening of the AuNP SPR absorption peak. Initially, the limited spectral overlap between AuNP absorption and AuNC emission results in a weak IFE, leading to strong red fluorescence from the AuNCs. Following AuNP aggregation, the enhanced spectral overlap induces significant IFE-mediated quenching of AuNC fluorescence, resulting in a pronounced decrease in the red emission intensity (Fig. 4). Thus, the ratio of the fluorescence intensity of red-emitting AuNCs to that of blue-emitting B-CDs serves as a reliable readout for quantifying the UO_2^{2+} concentration.

Quantum dots inherently lack affinity for UO_2^{2+} ions, necessitating surface modification with functional groups, such as carboxyl, pyridyl, or thiol, to enable selective binding. While quantum dots alone exhibit strong fluorescence, coordination with UO_2^{2+} leads to the formation of a non-emissive ground-state complex, resulting in fluorescence quenching through a static mechanism.[70] Zheng *et al.*[71] introduced abundant oxygen- and nitrogen-containing groups onto molybdenum oxide (MoOx) quantum dot surfaces, producing dopamine-functionalized molybdenum oxide quantum dots (DA-MoOx QDs) with high affinity for UO_2^{2+}. Upon coordination, these DA-MoOx QDs aggregated into larger clusters, which cause significant fluorescence quenching.

2.4 DNAzymes

DNAzymes are catalytic DNA molecules capable of specifically cleaving substrate strands upon activation by target metal ions, exhibiting high selectivity in recognition. This property makes DNAzymes ideal for the development of sensitive and selective sensors for UO_2^{2+} detection.[72]

2.4.1 DNAzymes for UO_2^{2+} detection. DNAzymes, functional nucleic acids, typically consist of a catalytic "enzyme strand" and a complementary "substrate strand". The enzyme strand catalyzes sequence-specific cleavage at a critical adenosine ribonucleotide site on the substrate strand upon activation by UO_2^{2+}.[73] Leveraging this recognition mechanism, fluorescent sensors can be constructed by labeling the DNA termini or specific bases with fluorophores and quenchers to create a reversible "signal switch". To enhance sensitivity, DNA self-assembly-based signal amplification strategies are employed. The initial UO_2^{2+}-triggered cleavage releases a primer that initiates cascade hybridization reactions, assembling large DNA nanostructures. This process spatially separates fluorophores and quenchers on a large scale, converting a single molecular event into amplified fluorescence output for sensitive UO_2^{2+} detection.[74] Chen *et al.*[75] developed an ultrasensitive DNA network fluorescence biosensor, in which UO_2^{2+}-activated DNAzyme cleavage releases trigger strands that initiate cyclic assembly of dual-hairpin probes (Hab, Hbc, and Hca), forming extensive DNA networks. This separates fluorophore (FAM) and

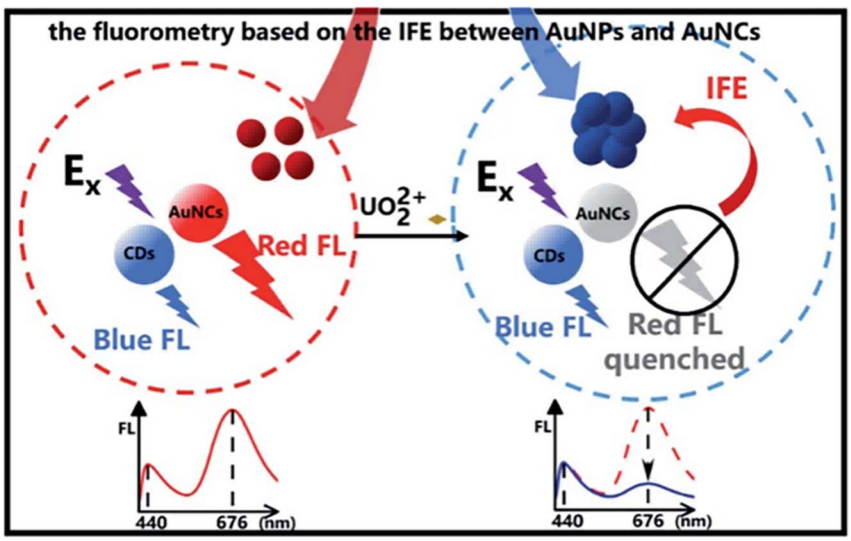

Fig. 4 Schematic of the IFE-based ratiometric fluorescence method for UO_2^{2+} detection. Reproduced with permission from ref. 69. Copyright 2022, the Royal Society of Chemistry.

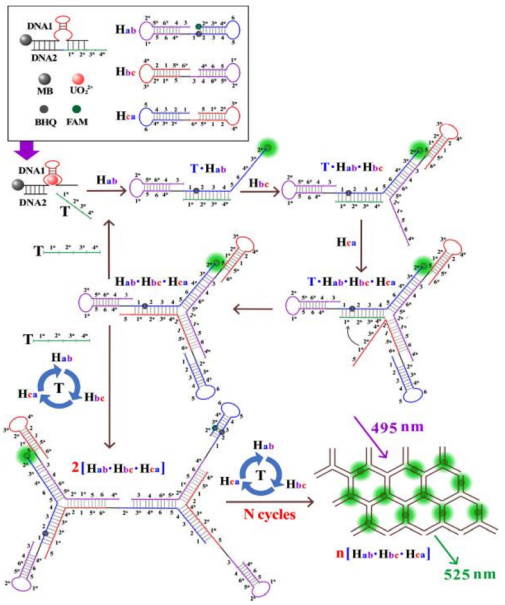

Fig. 5 Detection mechanism of the DNA network biosensor for the ultrasensitive detection of UO_2^{2+} based on the double-loop hairpin probe assembly. Reproduced with permission from ref. 75. Copyright 2024, the American Chemical Society.

quencher (BHQ) labels, yielding a markedly enhanced fluorescence signal with a detection limit down to 2 pM (Fig. 5). The sensor demonstrated high selectivity and precision in complex water and soil matrices. Lin *et al.*[76] reported a simplified DNA fluorescence sensor based on a single hairpin self-assembly chain reaction. Here, a palindrome-containing hairpin probe undergoes cyclic assembly, triggered by the DNAzyme-activated release of primer strands, forming fluorescent DNA nanowires. Compared to previous multi-hairpin DNA networks, this approach streamlines probe design and assay procedure without compromising sensitivity.

2.5 Comparison of properties between different materials

Table 1 summarizes the performance of representative materials selected from different categories for fluorescence-based UO_2^{2+} detection. Different materials exhibit distinct properties, which are inherently associated with variations in their molecular and structural characteristics. Analyzing the structure–property relationship enables us to design materials with superior performance.

Under acidic to neutral conditions, UO_2^{2+} remains the dominant form that can undergo cation exchange and directly coordinate with most binding sites. At pH > 7, it predominantly exists as the highly stable anionic complex $[UO_2(CO_3)_3]^{4-}$, which can cause materials and sensors originally designed to capture UO_2^{2+} to lose function entirely, especially those with anionic frameworks, such as MOFs and COFs.[77] As illustrated in Table 1, the optimal detection pH for most materials ranges from 3 to 7, which corresponds to the favorable speciation of UO_2^{2+}. Anionic MOFs perform well under mildly acidic conditions; however, extreme acidity or alkalinity can impair detection performance and damage MOF structures, attributed to the inherent lability of coordination bonds. Many MOF ligands contain nitrogen-containing moieties (*e.g.*, imidazole or pyridine) or oxygen-containing groups (*e.g.*, carboxyl groups). Excessive proton concentrations compete with UO_2^{2+} for binding sites and can protonate the ligands, thereby disrupting the coordination framework. Under alkaline conditions, hydroxide ions induce hydrolysis of metal nodes (*e.g.*, zinc or copper ions), resulting in framework collapse.[78] Compared to MOFs, COFs exhibit superior stability, due to their entirely organic frameworks and strong covalent bonds.[79] Fluorescent nanomaterials, such as metal nanoclusters and quantum dots, are susceptible to structural damage under extreme pH conditions: ligands on metal nanoclusters may undergo protonation or hydrolysis, while quantum dot nanocrystals are prone to corrosion, both of which lead to irreversible fluorescence loss. DNAzymes are particularly sensitive to extreme pH, as hydrolysis of purine bases or phosphodiester bonds disrupts their precisely folded three-dimensional structures, resulting in denaturation and the loss of both catalytic activity and specific UO_2^{2+} recognition capability.

The fluorescence response time is a key parameter that reflects the sensing efficiency of a material. As shown in Table 1, few studies on MOFs report clear fluorescence response times, whereas COF-based sensors generally exhibit rapid responses, with the majority achieving signal stabilization within 2 seconds. Both COFs and MOFs detect UO_2^{2+} through specific coordination between the uranyl ion and functional groups on their pore walls; this coordination event triggers electron transfer and energy-level transitions, which in turn alter the fluorescence properties of the materials. This rapid physicochemical interaction typically reaches equilibrium within a few seconds to one minute. The fluorescence of nanomaterials is intrinsic to their structure, and fluorescence quenching occurs promptly once UO_2^{2+} diffuses to the nanomaterial surface *via* collisions or weak coordination interactions. However, reported response times vary widely, ranging from 0.5 seconds to several minutes, depending on the experimental setup. For instance, UO_2^{2+}-induced the aggregation of AuNPs requires a certain amount of time to form stable clusters—a process that is essential for achieving significant and stable ratiometric fluorescence detection based on the IFE. Thus, the response speed of such sensors is constrained by the kinetics of AuNP aggregation. In contrast, DNAzyme-based sensors exhibit longer response times, ranging from tens of minutes to hours, due to their multistep catalytic processes, which involve UO_2^{2+} binding, conformational changes of the DNAzyme, and catalytic activity. Unlike porous materials (*e.g.*, MOFs and COFs) that possess large specific surface areas and multiple binding sites, a single DNAzyme molecule typically contains only a few catalytic sites, resulting in relatively lower sensing efficiency.

The detection limit is defined as the lowest concentration of UO_2^{2+} that can be reliably quantified, with lower detection limits indicating higher sensing sensitivity of the material. As shown in Table 1, MOFs exhibit linear detection ranges spanning one to five orders of magnitude, with detection limits ranging from several nanomolar to several micromolar. Their

Table 1 Comparison of the properties of different materials for the fluorescence detection of UO_2^{2+}

Material type	Material name	pH	Response time	Linear range (μM)	LOD (nM)	Ref.
MOFs	Tb-MOF	4	—	0.74–1296	3.33	80
	HNU-50	3	—	0.01–1000	12	52
	CSMCRI-21	5	20 s	1.26–1680	130	81
	Eu^{3+}@UiO-67-bpydc	6	—	0.01–0.1	3	54
	IRMOF-3-DPC	4	—	26.25–1260	1510	82
	Eu-DATP	—	—	0.01–100	2.7	55
COFs	TFPT-BTAN-AO	6	2 s	0.02–6	6.7	62
	TP-COF-AO	6	2 s	0–10	8.3	83
	PyTT-Tp	5	2 s	0.015–4.5	4.92	84
	TAPM-DHBD	5	2 s	0.01–3.7	4.08	28
	GC-TFPB-AO	7	—	0.05–0.5	21.25	63
Nanomaterials	AuNCs@AuNPs@B-CDs	2.5	12 min	0.2–5	8.4	69
	DA-MoOx QDs	6	5 min	0.005–1	3.85	71
	CMH-NCDs	4–5	0.5 s	0–20	8.4	85
DNAzymes	DNA network biosensor	6.6	100 min	0.00001–1	0.002	75
	DNA@SYBR green I	7.4	20 min	0.01–1	4.6	86
	DNA hairpin@39E DNAzyme	5.5	50 min	0.00005–0.02	0.017	76

porous structure provides abundant binding sites that resist rapid saturation, thereby yielding relatively wide linear ranges; however, the upper limit of these ranges is constrained by the diffusion rate of UO_2^{2+} within the pores. The strong coordination between UO_2^{2+} and high-affinity functional groups on MOFs enables these materials to achieve low detection limits. In comparison, COFs typically exhibit linear detection ranges of one to two orders of magnitude and detection limits ranging from several to tens of nanomolar. Despite possessing more stable covalent bonds and open pore structures than MOFs, the performance of COFs is similarly limited by the diffusion of UO_2^{2+} within their pores. Nanomaterials display linear detection ranges of one to three orders of magnitude, with detection limits generally in the single-digit nanomolar range. Their nanoscale dimensions confer high fluorescence efficiency and a large specific surface area, leading to excellent sensing sensitivity; however, the limited number of surface binding sites restricts their linear ranges due to facile saturation. DNAzymes offer linear detection ranges spanning two to five orders of magnitude and detection limits ranging from picomolar to nanomolar levels. The catalytic amplification effect and high specificity of aptamer-UO_2^{2+} binding allow a single UO_2^{2+} ion to trigger significant signal changes, resulting in ultralow detection limits.

2.5.1 Improvement in fluorescence performance. The core of fluorescence-based detection lies in the intensity and stability of the fluorescence signal, which are fundamentally dependent on the excellent luminescent properties of the sensing material.

For ligand-based luminescent MOFs, the selection of ligands with AIE properties offers distinct advantages. Such ligands exhibit weak fluorescence in their monomeric state but display significantly enhanced emission when confined within the fixed, ordered framework of MOFs. For metal-centered luminescent MOFs, the careful selection of organic ligands is critical to match their triplet energy levels with those of lanthanide ions (*e.g.*, Eu^{3+} and Tb^{3+}), thereby enabling efficient energy transfer. Alternatively, strong fluorophores, such as organic dyes or quantum dots, can be post-synthetically grafted onto MOF pores or frameworks to serve as new emission centers. For instance, Ahmad *et al.*[88] utilized ZIF-8 as a porous host to uniformly disperse quantum dots within its channels, which effectively suppressed aggregation, maintained high fluorescence efficiency, and consequently enhanced the photoluminescence quantum yield. Cui *et al.*[89] fabricated a composite of Tb-MOF and terbium alginate hydrogel (Tb-AG); this composite improved material stability and provided additional coordination sites for uranyl ions *via* the carboxyl oxygen atoms in Tb-AG, thereby greatly enhancing fluorescence quenching efficiency and achieving both high sensitivity and stability. COFs generally exhibit weaker fluorescence compared to MOFs, as dynamic covalent bonds facilitate nonradiative decay pathways. The introduction of lanthanide ions coordinated to COFs can act as antenna moieties, transferring absorbed energy from the organic framework to amplify the characteristic emission of lanthanides and dramatically improve the fluorescence performance. Mao *et al.*[90] coordinated Eu^{3+} to the nitrogen atoms in the bipyridine units within the COF, which restricted the free rotation of bipyridine and suppressed nonradiative energy dissipation caused by intramolecular rotation. This modification significantly enhanced the intrinsic fluorescence of the COF and enabled turn-on fluorescence detection of uranyl ions *via* resonance energy transfer. Similar to MOFs, post-synthetic modification can incorporate highly emissive molecules into COF pores, leveraging confinement effects to protect and enhance luminescence. For quantum dots, surface modification with organic molecules or polymers can improve their dispersibility and stability while reducing nonspecific interactions that induce fluorescence quenching. The introduction of heteroatom dopants (*e.g.*, nitrogen or sulfur) modifies their electronic structure, allowing for the tuning of emission color and enhancement of fluorescence intensity. Yang *et al.*[91] employed a ligand exchange strategy to functionalize originally hydrophobic CdSe/CdS/ZnS quantum dots, successfully converting them into water-soluble fluorescent

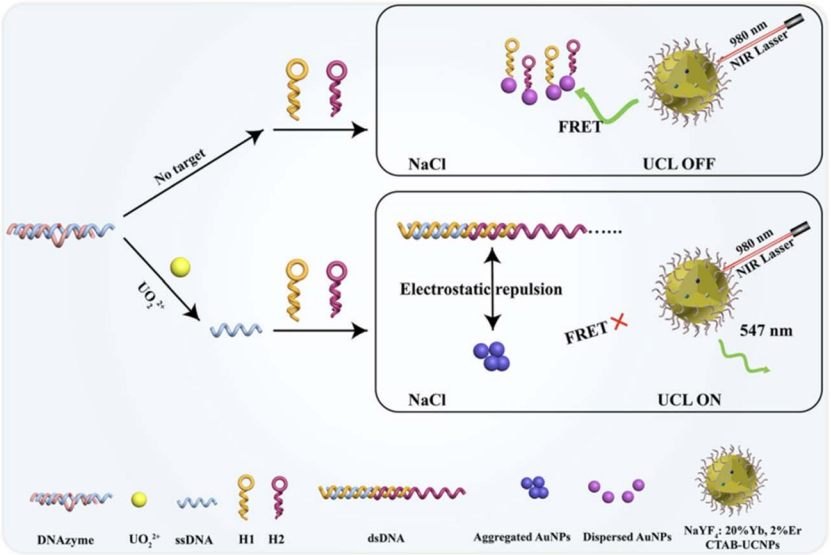

Fig. 6 Upconversion fluorescence platform for the sensitive quantification of UO_2^{2+} based on specific DNAzyme-mediated signal amplification and fluorescence resonance energy transfer. Reproduced with permission from ref. 87. Copyright 2024, Springer.

probes with excellent dispersibility and fluorescence properties. In the design of DNAzyme-based fluorescent sensors, the selection of high-performance fluorophores or integration with fluorescent materials enables highly specific detection. Zhang *et al.*[87] developed a "switch-on/off" fluorescent sensing platform by integrating upconversion nanoparticles (UCNPs), AuNPs, DNAzyme, and hybridization chain reaction (HCR). Specifically, UCNPs serve as energy donors and AuNPs as energy acceptors: in the absence of UO_2^{2+}, AuNPs remain dispersed and quench UCNPs' fluorescence *via* FRET, putting the system in an "off" state. Upon the introduction of UO_2^{2+}, the target ion triggers DNAzyme hydrolysis to produce single-stranded DNA (ssDNA), which further initiates HCR for the formation of long-chain double-stranded DNA (dsDNA). The electrostatic repulsion between dsDNA and AuNPs then induces AuNP aggregation, which weakens FRET and enables the subsequent fluorescence recovery of UCNPs (*i.e.*, an "on" state) (Fig. 6). This system synergistically combines the high specificity of DNAzyme-based recognition, the robust signal amplification of HCR, the low-background advantage of UCNPs, and the efficient quenching capability of AuNPs, thereby achieving ultrasensitive, highly selective, and rapid detection of UO_2^{2+}.

In summary, single materials often struggle to simultaneously achieve high fluorescence intensity and excellent stability. The key to performance enhancement lies in the strategic integration of complementary material properties through sophisticated composite design.

3. Colorimetry

Colorimetric detection is an analytical technique based on detectable color changes in a solution. It enables direct visual readout, facilitating rapid on-site screening and straightforward semi-quantitative assessment (Fig. 7).[92]

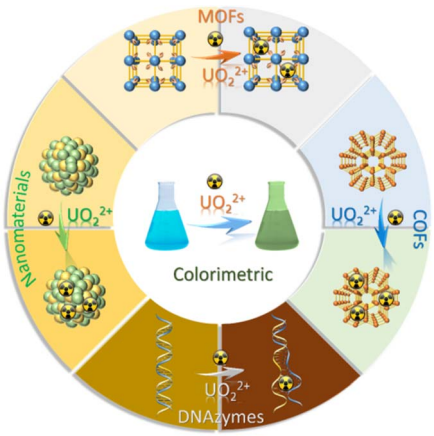

Fig. 7 Schematic of the colorimetric detection of UO_2^{2+} with different materials.

3.1 MOFs

The colorimetric detection of UO_2^{2+} based on MOFs relies on the catalytic reaction between MOF-enzyme composites and substrates, which induces a color change. The binding of UO_2^{2+} to the MOF-enzyme composite inhibits the enzyme's catalytic activity, preventing substrate oxidation and enabling colorimetric detection of uranyl ions.[93] In 2022, Zhou *et al.*[94] embedded hemin into two-dimensional ZIF-L nanosheets to form a biomimetic peroxidase, ZIF-L-hemin (Fig. 8). In the presence of H_2O_2, the composite catalyzes the oxidation of 3,3′,5,5′-tetramethylbenzidine (TMB), producing blue-colored oxidized TMB (oxTMB). Upon UO_2^{2+} introduction, coordination between U–N and the electron-rich 2-methylimidazole in ZIF-L disrupts the axial electron donation from imidazole to hemin-Fe, inhibiting the catalytic cycle. This results in

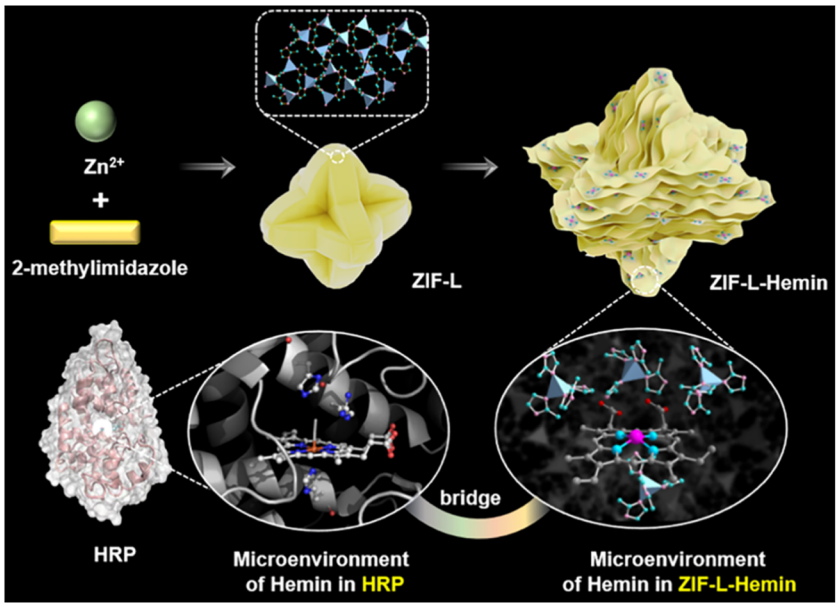

Fig. 8 Schematic of the synthesis procedure of ZIF-L-hemin and the structures of HRP and ZIF-L-hemin. Reproduced with permission from ref. 94. Copyright 2022, the American Chemical Society.

a decreased oxTMB yield and a color shift from deep blue to light blue or colorless.

3.2 COFs

The colorimetric method is based on the generation of highly reactive free radicals or reactive oxygen species on the surface of COF materials under light irradiation, which catalyze the substrate's colorimetric reaction.[95] The introduction of UO_2^{2+} inhibits this catalytic process through interactions with the COFs or the substrate. Xu *et al.*[96] developed a visible-light-responsive sulfone-based COF (TAS-COF) that exhibits oxidase-like activity upon visible-light excitation, catalyzing the conversion of the colorless substrate TMB into blue oxTMB. The imine groups in oxTMB coordinate with UO_2^{2+} to form a colorless complex, causing the fading of the blue color in the presence of uranyl ions (Fig. 9). Thus, monitoring the significant absorbance changes of the TAS-COF-TMB system enables sensitive colorimetric detection of UO_2^{2+}.

3.3 Nanomaterials

AuNPs can be employed to design colorimetric sensors for UO_2^{2+} detection. When dispersed, AuNPs exhibit strong absorption at a characteristic wavelength and reflect or scatter the complementary light, resulting in a distinct color. Upon aggregation, the plasmon coupling between particles induces a red shift in the localized surface plasmon resonance (LSPR) absorption peak, causing the solution color to change due to the absorption of longer-wavelength light.[97] Since AuNPs lack inherent specificity, their surfaces are functionalized with ligands that selectively coordinate to UO_2^{2+}. The binding of UO_2^{2+} to these ligand crosslinks dispersed AuNPs into larger aggregates, triggering a visible color transition. Zhang *et al.*[98] functionalized AuNPs with phosphate groups, imparting a negative charge and yielding a stable wine-red colloidal solution. Specific coordination between UO_2^{2+} and the phosphate groups reduces the electrostatic repulsion among the AuNPs, inducing nanoparticle aggregation. This shifts the SPR peak from 519 nm to approximately 650 nm, with the solution color changing from wine red to blue, enabling sensitive colorimetric detection of UO_2^{2+}.

3.4 DNAzymes

In the presence of UO_2^{2+}, DNAzymes specifically cleave their substrate and form peroxidase-mimicking DNAzyme complexes that catalyze the oxidation of chromogenic ions in solution, causing a visible color change for detection.[29] Zhang *et al.*[99] developed a colorimetric assay combining DNAzyme-modified agarose microbeads with cascade signal amplification for UO_2^{2+} detection. A bifunctional DNA probe integrates a uranyl-specific DNAzyme substrate as the recognition element and a rolling circle amplification (RCA) primer as the signal transducer, immobilized on MBs *via* the biotin–streptavidin interaction. Upon UO_2^{2+} addition, the DNAzyme cleaves the substrate strand, releasing the primer to initiate RCA, producing abundant guanine quadruplex (G-quadruplex) repeats. The G-quadruplexes complex with hemin to form peroxidase-like catalysts that oxidize $ABTS^{2-}$ with H_2O_2, generating a blue-green color detectable by the naked eye or UV-vis spectroscopy (Fig. 10).

3.5 Comparison of properties between different materials

For the currently reported colorimetric detection of UO_2^{2+} using MOFs, COFs, and DNAzymes, the underlying principle is uniformly based on enzyme-catalyzed oxidation or inhibition

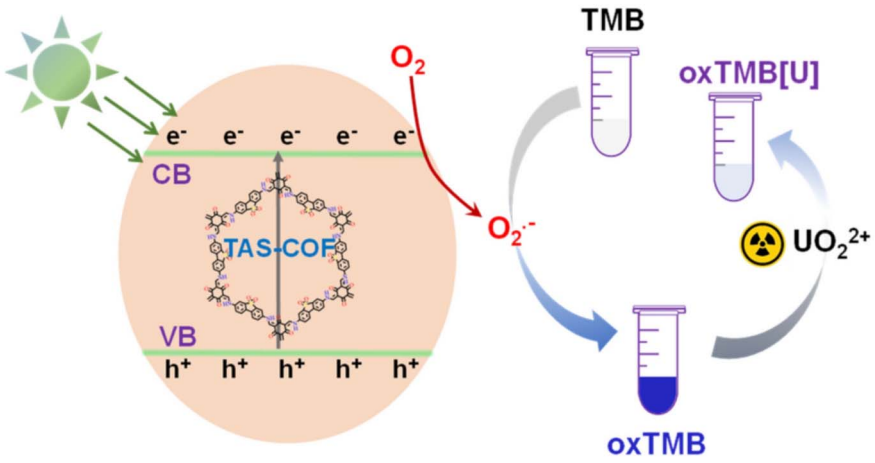

Fig. 9 Illustration of the colorimetric detection of UO_2^{2+} using visible-light-responsive TAS-COF. Reproduced with permission from ref. 96. Copyright 2022, MDPI.

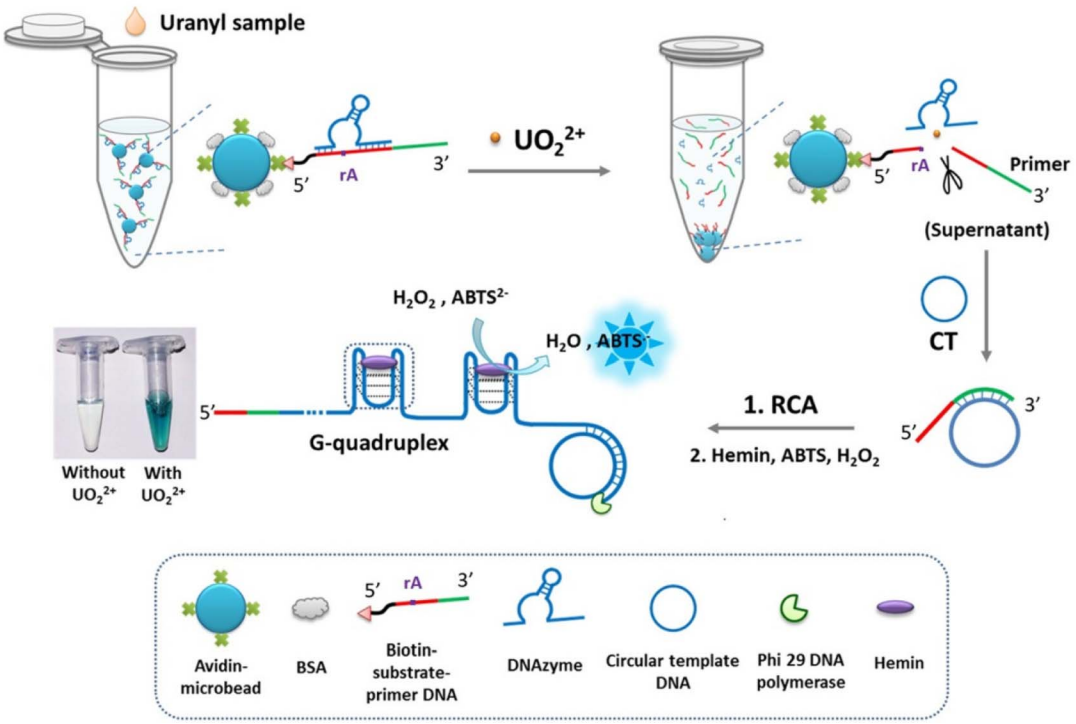

Fig. 10 Schematic of the DNAzyme colorimetric detection of UO_2^{2+}. Reproduced with permission from ref. 99. Copyright 2022, the Royal Society of Chemistry.

events that modulate substrate conversion, thereby inducing a color change. The final colorimetric signal is derived from the oxidized product of the substrate, whose chemical structure and absorption maximum are typically governed by the pH condition. Colorimetric detection is usually performed under fixed pH conditions, as pH affects not only the structural stability of the materials but also the catalytic activity of enzymes and the stability of substrates involved in the colorimetric reaction. Therefore, maintaining an optimal pH to ensure maximum catalytic activity and the formation of a stable, intensely colored product is crucial for achieving high-sensitivity detection.

As shown in Table 2, MOF-based colorimetric sensors exhibit the fastest response, whereas DNAzyme-based assays require the longest response time. This striking difference in response kinetics can be fundamentally attributed to the distinct nature of their catalytic systems. Although MOF, COF, and DNAzyme-based methods all rely on enzyme-mimetic catalyses, the catalytic activity of MOFs and COFs originates from the materials themselves, which act as abiotic nanozymes rather than fragile

Table 2 Comparison of the properties of different materials for the colorimetric detection of UO_2^{2+}

Material type	Material name	pH	Response time	Linear range (μM)	LOD (nM)	Ref.
MOFs	ZIF-L-hemin	7	3 min	0.25–40	79	94
COFs	TAS-COF	3.5	10 min	0.25–25	70	96
	JUC-505-AO	5.6	25 min	0–20	148	17
Nanomaterials	VPA-AuNPs	—	9 min	0.5–10	1070	98
DNAzymes	Bifunctional DNA probe	5.5	40 min	0.001–0.05	0.48	99

biological enzymes. Unlike natural enzymes that require strict conformational maintenance to retain activity, these porous framework materials possess inherent, structure-dependent catalytic active sites (*e.g.*, metal nodes and functionalized organic linkers) that enable direct, unimpeded substrate access and rapid redox reactions. Consequently, their catalytic efficiency and reaction rate are generally more stable than those of biological enzymes, leading to significantly faster colorimetric responses. In contrast, DNAzyme-based colorimetric detection involves a multistep biological catalytic process, including UO_2^{2+}-dependent substrate cleavage, G-quadruplex formation, and subsequent peroxidase-mimetic catalysis for substrate oxidation. Each step in this cascade requires sufficient time for molecular recognition, conformational rearrangement, and catalytic turnover, which inherently prolongs the overall reaction time and results in the slowest response among the studied methods. Notably, AuNP-based colorimetric sensors do not rely on enzymatic catalysis; instead, they leverage LSPR changes induced by physical and chemical interactions, enabling rapid color transitions driven by direct nanoparticle aggregation without catalytic lag.

Regarding detection sensitivity, the DNAzyme-based method achieves an exceptionally low limit of detection (LOD), far outperforming MOF-, COF-, and AuNP-based sensors, while AuNP-based sensors exhibit the highest LOD. This performance gap arises directly from the fundamental differences in their sensing mechanisms. The DNAzyme-based colorimetric method for UO_2^{2+} detection capitalizes on its high specificity to UO_2^{2+}, which enables precise, signal-amplified catalytic turnover even at ultratrace analyte concentrations. Each UO_2^{2+} ion can trigger the cleavage of multiple DNAzyme substrates, initiating a cascade of G-quadruplex formation and peroxidase-mimetic catalysis that amplifies the colorimetric signal exponentially, thus enabling detection at sub-nanomolar levels. In contrast, the use of AuNPs results in a relatively higher detection limit. This is because the underlying mechanism requires a sufficient concentration of UO_2^{2+} to neutralize the abundant negative charge on the AuNP surface, thereby overcoming electrostatic repulsion and triggering nanoparticle aggregation, which is accompanied by a subsequent color change. At low UO_2^{2+} concentrations, only limited aggregation occurs, producing a color change too weak to be reliably detected by either the naked eye or analytical instruments. Additionally, AuNP aggregation is a non-catalytic, stoichiometric process with no signal amplification, further limiting its sensitivity compared to catalytically amplified methods.

For MOF and COF-based sensors, their LOD values fall between those of DNAzyme- and AuNP-based sensors, which can be explained by their intermediate catalytic amplification and binding affinity. As porous framework nanozymes, MOFs and COFs offer moderate catalytic activity and UO_2^{2+} adsorption capacity, enabling signal amplification through catalytic substrate oxidation; however, they lack the extreme specificity and exponential amplification capability of DNAzyme systems. This balance results in sensitivity that is higher than those of AuNP-based aggregation sensors but lower than those of DNAzyme-based assays, aligning with the trend observed in Table 2.

3.5.1 Improvement in colorimetric detection performance. Currently, reports on the colorimetric detection of UO_2^{2+} remain limited. Colorimetric sensors based on MOFs, COFs, and nanomaterials rely on enzyme–substrate catalytic reactions to generate changes in a single signal unit, lacking effective signal amplification mechanisms; this limitation hinders the detection of ultra-low UO_2^{2+} concentrations. Additionally, the intrinsic color and turbidity of the solution, as well as the presence of other colored substances in the sample, can directly interfere with absorbance measurements, thereby compromising the accuracy and reliability of the detection results.

The sensitivity of UO_2^{2+} detection can be improved by enhancing the intrinsic selectivity of the sensing material. Materials, such as MOFs, COFs, and nanomaterials, can be modified through post-synthetic incorporation of specific functional groups, including amidoxime or phosphate groups, which exhibit strong coordination affinity toward UO_2^{2+}. These optimized materials can be integrated with smartphone platforms, yielding more objective and quantifiable results compared to visual observation and enabling a transition from qualitative to semiquantitative analysis. This integrated approach facilitates rapid, on-site, and equipment-free quantitative detection, significantly improving the practicality and accessibility of UO_2^{2+} monitoring. For instance, Lei *et al.*[100] developed a convenient and portable smartphone-assisted colorimetric method for UO_2^{2+} detection. Rifampicin and Br-PADAP were used as chromogenic agents, which undergo coordination reactions with UO_2^{2+} separately, resulting in distinct color changes of the solutions: from orange to dark red in the rifampicin system and from yellow to light pink in the Br-PADAP system. As illustrated in Fig. 11, a custom colorimetric viewfinder was employed to standardize the smartphone's shooting conditions; digital images of the reacted solutions were then imported into the built-in "Detect" application to extract the S value (saturation) of HSV and the L value

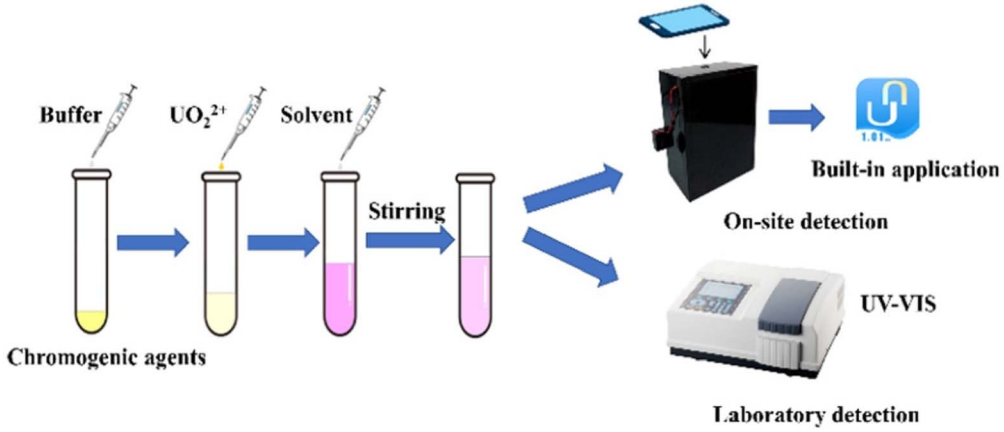

Fig. 11 Schematic of the chromogenic reactions for the detection of UO_2^{2+}. Reproduced with permission from ref. 100. Copyright 2023, the Royal Society of Chemistry.

(lightness) of HSL. Leveraging the linear relationships between these color parameters and the UO_2^{2+} concentration, on-site rapid estimation of the concentration range was achieved. Meanwhile, combined with the characteristic peak detection using a UV-vis spectrophotometer at 375 nm (rifampicin system) and 562 nm (Br-PADAP system), precise quantification with a low limit of detection of 0.89 μM was realized. This platform integrates a dual-mode of "on-site preliminary screening and laboratory precise determination", which not only addresses the timeliness requirement of on-site emergency detection but also ensures the accuracy of laboratory analysis, achieving the unification of "portability" and "precision".

4. Electrochemical detection

Electrochemical detection is a sensitive and selective detection method for trace UO_2^{2+}, which involves measuring the current signal generated by the redox reaction of UO_2^{2+} on the electrode surface, facilitated by high-sensitivity pulse voltammetry and a functional electrode-modified interface (Fig. 12).[32]

4.1 MOFs

MOFs provide well-defined pores and high specific surface areas, and, upon carbonization, they form conductive three-dimensional networks.[101] The resulting MOF-derived porous carbon materials possess negatively charged surfaces that strongly attract the positively charged UO_2^{2+} ions in solution, enabling efficient enrichment of UO_2^{2+} at the electrode interface. This facilitates the electrochemical reduction of UO_2^{2+} on the electrode surface, producing measurable reduction currents for uranium detection.[102] In 2020, Cao *et al.*[103] used UiO-66-NH_2 as a precursor to embed PtRu bimetallic nanoparticles onto MOF-derived porous carbon to create a composite for electrochemical UO_2^{2+} detection (Fig. 13). The embedded PtRu nanoparticles serve as key catalytic centers, significantly lowering the overpotential required for UO_2^{2+} reduction and accelerating electron transfer. The porous carbon provides a large surface area and rapid electron- and ion-transport channels, greatly amplifying the current signal. The synergistic interaction between PtRu nanoparticles and MOF-derived porous carbon enhances the overall electrochemical performance.

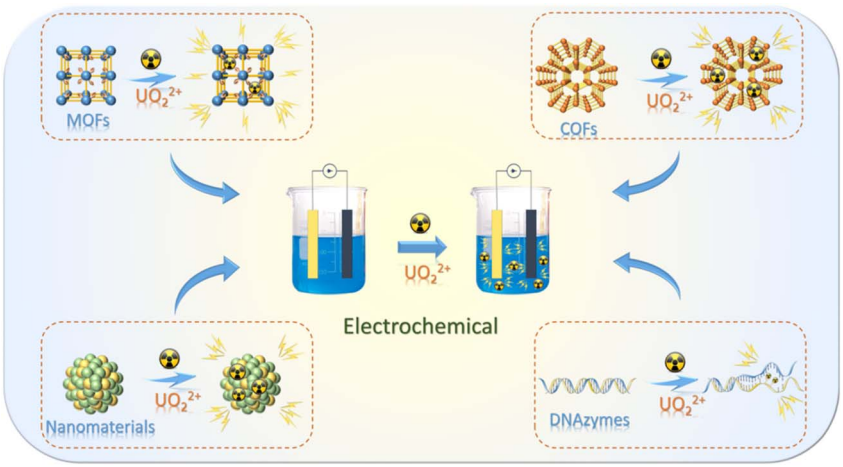

Fig. 12 Schematic of the electrochemical detection of UO_2^{2+} with different materials.

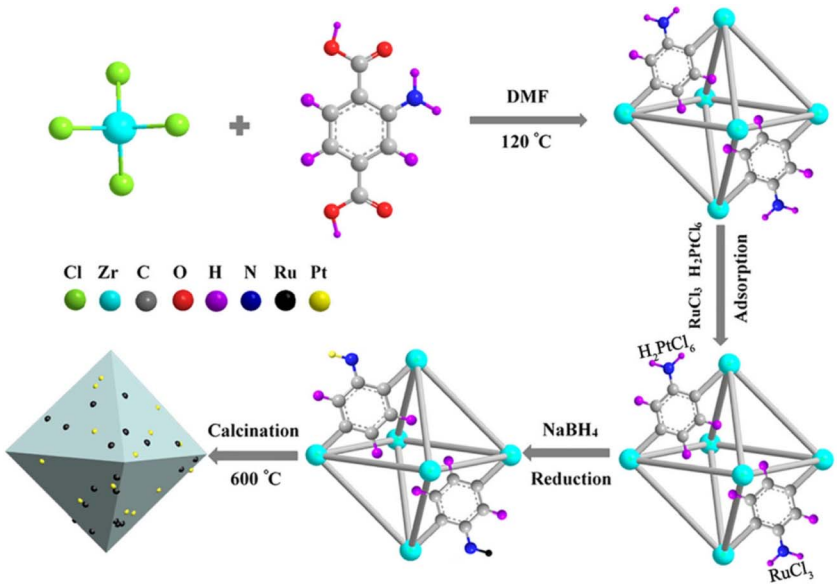

Fig. 13 Schematic of the synthesis of Pt_1Ru_2-PC. Reproduced with permission from ref. 103. Copyright 2020, Springer.

4.2 COFs

COFs can be employed for electrochemiluminescence (ECL) detection of UO_2^{2+}, a technique that integrates electrochemical reactions with optical signal measurement. By rational design and the selection of electron donor and acceptor units within COFs, efficient intramolecular charge transfer (ICT) can be achieved, exciting electrons in the COF to produce luminescence. Specific binding of UO_2^{2+} to functional groups in the COF alters its electronic structure, thereby modulating the ECL intensity.[104] Cui *et al.*[105] developed an alkene-linked COF, TBTN-COF, and synthesized a BCBA-TBTN-AO complex by converting cyano groups in the COF into amidoxime groups, enabling selective UO_2^{2+} coordination. Although the monomers are non-luminescent, the ICT within the framework induces strong ECL, where TBTN serves as the electron acceptor and BCBA and DAFB as electron donors, facilitating effective charge transfer. Under applied potential, the electrons in the COF are excited to form radical anions, which emit light upon collision with superoxide anions, generating a robust ECL signal (Fig. 14). The coordination of UO_2^{2+} with BCBA-TBTN-AO transfers electrons from the donor units to TBTN, enhancing the ECL response and establishing a highly selective "turn-on" ECL sensing system with ultralow detection limits.

4.3 Nanomaterials

Nanomaterials, featuring a high specific surface area, abundant active sites, and excellent conductivity, serve as carriers to immobilize numerous recognition elements and establish efficient electron-transfer channels with electrodes, enabling highly sensitive detection of low-concentration uranyl ions.[106] Han *et al.*[107] modified a glassy carbon electrode (GCE) with AuNPs for uranium detection using differential pulse adsorptive stripping voltammetry. Distinct redox peaks were observed on all electrodes. After the AuNP modification, the oxidation peak current increased from 454 μA to 579 μA, corresponding to a 27.53% enhancement, which clearly demonstrates the superior electron-transfer capability of the AuNPs/GCE. In this method, UO_2^{2+} is first reduced and deposited onto the electrode at negative potentials. A subsequent positive potential scan then oxidizes and strips the deposited uranium, generating an oxidation peak current corresponding to the UO_2^{2+} concentration. The high surface area of AuNPs significantly increases the active electrode area, which amplifies the stripping signal and enhances the detection sensitivity.

4.4 DNAzymes

DNA itself is non-conductive; thus, to realize electrochemical detection, electroactive molecules are covalently attached at specific positions on the DNA strand, along with UO_2^{2+} binding aptamers.[108] When UO_2^{2+} binds to the aptamer, it induces conformational changes in the DNA structure. This conformational shift affects the electron-transfer efficiency between the electroactive molecule and the electrode, resulting in measurable current changes.[109]

Jett *et al.*[110] reported a DNA-based electrochemical biosensor for detecting UO_2^{2+} in water. The sensor employs a modified uranyl-binding aptamer embedded within an oligonucleotide scaffold, forming a reusable, conformation-switching electrochemical DNA biosensor (Fig. 15A). Upon UO_2^{2+} binding, the DNAzyme activity is triggered, causing cleavage at a specific site and a conformational switch from an unbound to a bound state (Fig. 15B). This structural change alters the position and environment of the methylene blue electroactive reporter attached to the DNA, thus modulating electron transfer at the electrode surface and generating a corresponding electrochemical signal change.

4.5 Comparison of properties between different materials

As shown in Table 3, distinct variations in electrochemical detection performance are observed across different material

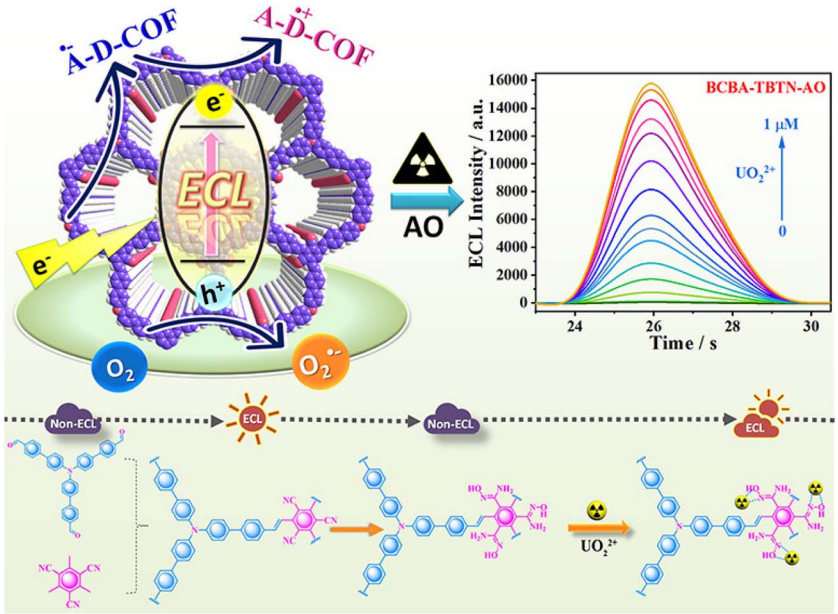

Fig. 14 Schematic of the COF-based electrochemiluminescence detection of UO_2^{2+}. Reproduced with permission from ref. 105. Copyright 2021, the American Chemical Society.

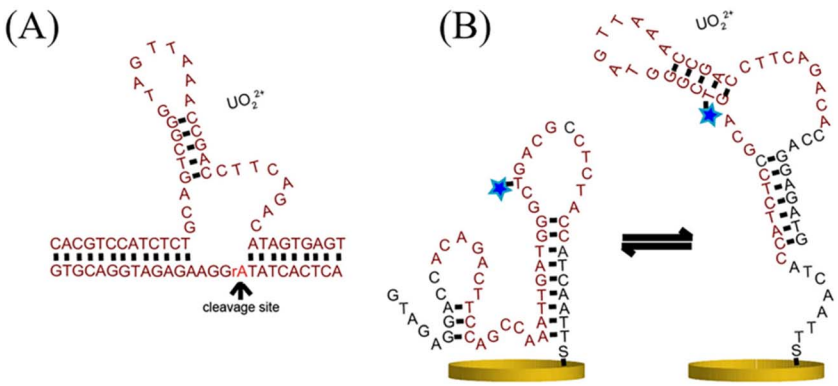

Fig. 15 (A) Schematic of the DNAzyme–UO_2^{2+} binding. Reproduced with permission from ref. 110. Copyright 2017, Wiley. (B) Schematic of the conformation-switching E-DNA uranyl biosensor. Reproduced with permission from ref. 110. Copyright 2017, Wiley.

systems for UO_2^{2+} analysis. Specifically, COFs and nanomaterials outperform MOFs and DNAzymes in terms of linear ranges and LOD values, while the latter two material categories are relatively less reported and typically exhibit inferior sensing metrics. This performance disparity stems fundamentally from the intrinsic electronic and structural properties of each material class, as well as their compatibility with electrochemical transduction mechanisms.

Most MOFs and COFs are inherently semiconductors or insulators with low electrical conductivity, which severely restricts efficient electron transfer between the electrode interface and the bulk of the material. This limitation directly translates into sluggish electron kinetics and weak signal generation, ultimately resulting in the relatively high LOD (24 nM) and narrow linear range (0.168–3.528 μM) observed for MOF-based sensors like PtRu–PCs (Table 3). In contrast, conductive nanomaterials, such as AuNPs and PNPs, possess exceptional electron mobility, large specific surface areas, and robust electrocatalytic activity. These features facilitate rapid electron transfer at the electrode surface, enabling wider linear ranges (*e.g.*, PNPs cover 0.00000037–0.00037 μM) and lower LOD values (*e.g.*, AuNPs/GCE at pH 3 achieves 0.44 nM). However, unmodified conductive nanomaterials lack specific recognition sites for uranyl ions, making them vulnerable to interference from coexisting ions and compromising detection selectivity—a critical drawback reflected in their limited practical applicability.

COFs bridge the gap between the low conductivity of pristine MOFs and the non-selectivity of bare nanomaterials. Their porous framework structure not only provides abundant active sites for UO_2^{2+} adsorption but also, when integrated with conductive components (*e.g.*, AuNCs@COF), increases electron-

Table 3 Comparison of the properties of different materials for the electrochemical detection of UO_2^{2+}

Material type	Material name	pH	Response time	Linear range (μM)	LOD (nM)	Ref.
MOFs	PtRu-PCs	4.6	3 min	0.168–3.528	24	103
COFs	AuNCs@COF	4	60 min	0.0005–25	0.347	111
	BCBA-TBTN-AO/GCE	5.5	150 s	0.000001–0.001	0.00036	105
Nanomaterials	AuNPs/GCE	3	600 s	0.0084–0.042	0.44	107
	AuNPs/GCE	1.6	400 s	0.010–0.20	1.26	112
	PNPs	7.4	—	0.00000037–0.00037	0.0021	113
DNAzymes	SG@dsDNA@$[Fe(CN)_6]^{3-/4-}$	5.5	75 min	0.001–1	0.13	114
	Electrochemical biosensor	5	—	0.1–500	1200	110

transfer efficiency. This synergy explains the superior performance of COF-based sensors: AuNCs@COF achieves an ultra-low LOD of 0.347 nM across a wide linear range (0.0005–25 μM), while BCBA-TBTN-AO/GCE sets an impressive LOD of 0.00036 nM (0.000001–0.001 μM). These results validate that combining COFs with conductive nanomaterials addresses the conductivity limitation of pure frameworks while retaining their specific recognition capability.

For DNAzyme-based electrochemical sensors, their poor performance (*e.g.*, SG@dsDNA@$[Fe(CN)_6]^{3-/4-}$ has an LOD of 0.13 nM and a narrow linear range of 0.001–1 μM) arises from the intrinsic electro inactivity of DNAzymes. Unlike catalytically active nanomaterials or semiconducting frameworks, DNAzymes lack inherent electron-transfer capacity; their signal transduction relies on UO_2^{2+}-induced DNA cleavage, which must be coupled with electroactive probes (*e.g.*, $[Fe(CN)_6]^{3-/4-}$) or conductive substrates to generate a measurable electrochemical response. This multi-step coupling process introduces additional barriers to electron transfer and signal amplification, resulting in relatively higher LODs and narrower linear ranges compared with those for COF and nanomaterial-based sensors. Even the electrochemical biosensor reference shows a high LOD of 1200 nM, further highlighting the challenges of direct electrochemical detection with unmodified DNAzymes.

In summary, the performance differences in Table 3 are tightly governed by the electronic conductivity, specific recognition ability, and structural synergy of each material system. Composite structures, combining porous MOFs/COFs with conductive nanomaterials or coupling DNAzymes with electroactive transducers, have emerged as a universal strategy to overcome intrinsic limitations, enabling high sensitivity and wide linear ranges for UO_2^{2+} electrochemical detection.

4.5.1 Improvement in electrochemical detection performance. MOFs carbonized at high temperatures can be converted into porous carbon materials with a high specific surface area. These carbonized materials not only retain the original porous structure of the parent MOF but also form an efficient three-dimensional conductive network, which greatly facilitates rapid electron transfer at the electrode surface. For COF materials, their overall electrical conductivity can be improved by introducing dopants or integrating conductive components to construct continuous conductive networks. Nanomaterials are commonly used as electrode modifiers to increase electron-transfer efficiency, and they are often combined with MOFs, COFs, DNAzymes, or functional groups with high affinity for UO_2^{2+} to improve detection selectivity and adsorption capacity. For example, Jiang *et al.*[115] first grafted amidoxime groups onto fluorinated graphene for the electrochemical detection of UO_2^{2+}. The two-dimensional layered structure of fluorinated graphene provides a large specific surface area for loading abundant amidoxime groups, which specifically bind to UO_2^{2+}, thereby enhancing sensor sensitivity and uranium enrichment efficiency. Chen *et al.*[116] developed a dual-signal amplification electrochemical platform by using gold nanoparticles as signal amplifiers and synthesizing silver nanoclusters *via* a hybridization chain reaction (HCR). The gold nanoparticles increased the loading of uranyl-specific DNAzymes on the electrode surface. In the presence of UO_2^{2+}, the DNAzyme is activated and cleaves the substrate strand, triggering the HCR, which generates long double-stranded DNA (dsDNA) on the electrode surface. This dsDNA acts as a template for the *in situ* synthesis of abundant silver nanoclusters, leading to significant amplification of the electrochemical signal.

5. Comparison of different detection methods

As shown in Table 4, a comprehensive performance comparison reveals that each detection method possesses distinct advantages and limitations, which are systematically summarized below.

Table 4 Performance comparison of different methods for detecting UO_2^{2+}

Detection method	Linear range	LOD	Selectivity	Convenience	Response time
Fluorescence	Ordinary	Low	High	Ordinary	Rapid
Colorimetry	Narrow	High	Ordinary	Excellent	Fast
Electrochemical detection	Wide	Extremely low	Ordinary	Limited	Moderate

Fluorescence-based detection exhibits a balanced profile, with superior sensitivity and selectivity. Through sophisticated probe design (*e.g.*, DNAzymes) and signal amplification strategies, it can achieve ultra-low LODs at the nanomolar to picomolar level. The high selectivity is inherently derived from the specific molecular recognition between uranyl ions and functional probes (*e.g.*, G-quadruplex structures or amidoxime groups), which effectively minimizes interference from coexisting ions. Operationally, this method offers convenience as it typically requires only sample-probe mixing without complex pretreatment, enabling quantitative analysis *via* fluorescence intensity changes. Kinetic studies benefit from the rapid response as fluorescence quenching or enhancement occurs instantaneously upon target binding, usually within minutes, facilitating real-time monitoring. However, its primary constraint lies in the reliance on sophisticated optical instrumentation (*e.g.*, fluorometers), which restricts its applicability for field-deployed, on-site rapid testing and confines it mainly to laboratory settings.

Colorimetric detection excels in terms of operational convenience and speed, marked as "Excellent" and "Fast" in Table 4, making it the preferred choice for naked-eye, on-site analysis. It delivers results within seconds to minutes through visible color changes. However, this convenience comes at the cost of sensitivity, characterized by a "High" LOD and a "Narrow" linear range. This performance trade-off stems from the fundamental mechanism: colorimetric signals rely on the accumulation of sufficient chromophores to produce a measurable absorbance change. At low concentrations, the signal is too weak to be detected, while at high concentrations, color saturation occurs, leading to a non-linear relationship between intensity and concentration. Furthermore, the method is highly susceptible to environmental interferences. Its "Ordinary" selectivity is attributed to the high pH sensitivity of the chromogenic reaction; even minor changes in pH or direct competition from other metal ions can alter the reaction equilibrium, resulting in false signals or background interference.

Electrochemical detection stands out with the highest sensitivity, featuring an "Extremely low" LOD and a "Wide" linear range (Table 4), making it ideal for trace-level analysis in complex matrices. This high sensitivity stems from its direct signal-transduction mechanism, in which trace UO_2^{2+} undergoes rapid redox reactions at the electrode surface and generates measurable current signals, while efficient electron transfer and interfacial signal amplification further lower the detection limit and extend the linear range. Despite these advantages, the method suffers from notable practical limitations: electrode modification typically involves complex, time-consuming assembly steps that demand skilled operation and yield unstable interfaces, resulting in "Limited" convenience. Its "Moderate" response time can be attributed to the necessary adsorption and accumulation of UO_2^{2+} prior to effective signal generation, and its reliance on costly, specialized potentiostats prevents truly portable and real-time field applications. Moreover, its "Ordinary" selectivity arises from the inherent nature of electrochemical transduction, as other redox-active metal ions can produce overlapping interfering currents or compete for active sites, making it difficult to achieve exclusive recognition of uranyl ions without highly specific functional modification.

In summary, Table 4 clearly delineates the performance spectrum: fluorescence offers high sensitivity and speed but requires lab equipment; colorimetry provides unmatched on-site convenience but sacrifices linear range and sensitivity; electrochemistry delivers ultra-sensitivity but lacks portability and simplicity. This comparison underscores the importance of tailoring method selection to specific application scenarios, whether prioritizing laboratory accuracy, field portability, or trace-level detection.

To address these performance trade-offs and achieve comprehensive detection capabilities, integrating multiple complementary techniques into a single platform has emerged as a promising strategy. This dual-modal approach not only leverages the strengths of individual methods but also mitigates their respective limitations, thereby significantly enhancing the overall reliability and practical applicability of the sensor. Chen *et al.*[111] developed an innovative dual-mode colorimetric and electrochemical sensor for UO_2^{2+} detection using AuNCs@COF composites (Fig. 16A and B). This material combines excellent electrocatalytic activity with optical properties, embedding nanoclusters with peroxidase-mimicking activity that catalyze substrates, inducing a color change in the presence of UO_2^{2+}. Simultaneously, the composite on the electrode catalyzes electrochemical reactions with UO_2^{2+} to generate current signals. Dual measurement of electrochemical and colorimetric signals allows mutual validation, improving accuracy and reliability. Xiong *et al.*[117] designed a fluorescence/colorimetric dual-mode sensing strategy based on cerium-sulfonated calix[4]arene (SC4A@Ce). This method cleverly exploits SC4A coordination with Ce^{3+} and Ce^{4+}: Ce^{3+} fluorescence is quenched when bound to SC4A but restored upon the addition of UO_2^{2+}, which

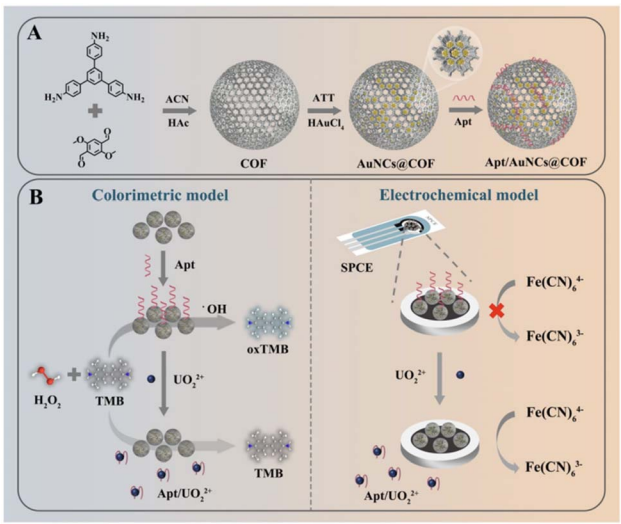

Fig. 16 (A) Preparation of COF, AuNCs@COF, and Apt/AuNCs@COF. Reproduced with permission from ref. 111. Copyright 2025, Springer. (B) Schematic of the principles of colorimetric and electrochemical dual-mode sensor detection of UO_2^{2+}. Reproduced with permission from ref. 111. Copyright 2025, Springer.

displaces Ce^{3+}. Meanwhile, Ce^{4+}'s oxidase-like activity catalyzes TMB oxidation to oxTMB, changing the solution color from blue to colorless. By combining highly sensitive fluorescence with visible colorimetric analysis, this approach achieves enhanced sensitivity, accuracy, and reliability. Wu *et al.*[118] developed a dual-mode colorimetric and photothermal sensor based on self-assembled TMB-CuO_2 nanosheets for UO_2^{2+} detection. In acidic environments, the nanosheets spontaneously decompose to generate Cu^{2+}, H_2O_2, and TMB *in situ*. A Fenton reaction then oxidizes TMB to blue oxTMB, which produces both a strong colorimetric signal and an efficient photothermal effect. UO_2^{2+} selectively coordinates with the imine groups of oxTMB. This coordination disrupts the conjugated structure of oxTMB, resulting in color fading, and simultaneously suppresses its photothermal conversion efficiency. Together, these effects produce a concentration-dependent dual signal response. By integrating the substrate, catalyst, and signal units into a single nanosheet without the need for external H_2O_2, this sensor achieves highly selective detection. It enables straightforward visual screening with the naked eye and on-site quantification based on thermal signal changes.

6. Summary and outlook

In summary, this review provides a comprehensive examination of recent advancements in materials research for the optical and electrochemical detection of UO_2^{2+}, with particular focus on MOFs, COFs, nanomaterials, and DNA-based materials. These materials offer distinct advantages in the selective and sensitive detection of UO_2^{2+}, contributing to the development of efficient monitoring platforms. Despite the remarkable breakthroughs achieved in this field, several challenges persist for the practical application of UO_2^{2+} detection.

6.1 Challenges in practical deployment

6.1.1 Complex matrix interference. Real-world uranium-contaminated samples are complex multi-component matrices, markedly different from the pure buffer solutions used in laboratory validation. Seawater, industrial wastewater, soil leachate and groundwater all contain coexisting ions, dissolved organic matter, humic acids and suspended particulates, which exert dual adverse effects on detection performance. These substances engage in non-specific binding with sensing materials, competing with UO_2^{2+} for active recognition sites, reducing detection selectivity, and inducing false positive or negative signals. They also cause physical and chemical interferences that disrupt signal transduction: dissolved organic matter absorbs excitation and emission light in fluorescence detection, exacerbating the inner filter effect, while suspended particulates induce turbidity in colorimetric assays and obscure visual and spectroscopic readouts. Electrochemical detection faces comparable vulnerabilities, as redox-active coexisting ions produce overlapping current signals at the electrode surface, and organic fouling of modified electrodes blocks active sites and impairs electron transfer. Seawater is a particularly critical matrix for marine uranium resource exploration and nuclear wastewater monitoring, and it poses an extreme challenge for detection systems. Its high salinity leads to electrostatic screening of charged recognition groups on sensing materials, severely weakening the binding affinity between sensing materials and UO_2^{2+}.

6.1.2 Field environmental stability issues. The structural and functional stability of sensing materials is a prerequisite for practical deployment, yet most state-of-the-art materials, including MOFs, COFs, DNAzymes and some nanomaterials, show poor stability under the harsh environmental conditions of real-world sampling sites. Porous MOFs are built on labile coordination bonds that hydrolyze or collapse under extreme pH and high ionic strength conditions, resulting in the loss of porous structure and recognition sites. COFs feature more robust covalent backbones, but their dynamic covalent bonds are prone to hydrolysis in aqueous environments during prolonged use, which impairs long-term stability. DNAzymes and nucleic acid-based sensors are highly sensitive to environmental factors; extreme pH, high temperature and nucleases in natural water bodies cause DNA denaturation and cleavage, leading to the loss of catalytic and recognition activity, which restricts their application in unprocessed natural samples. Even inorganic nanomaterials suffer from stability issues: surface ligand desorption in high-salinity solutions reduces their colloidal stability, and the oxidative corrosion of metal nanoparticles weakens their optical and electrochemical properties, giving rise to signal drift and poor reproducibility.

6.1.3 Instrumentation and operational limitations for on-site detection. On-site, real-time and portable monitoring stands as a key goal for UO_2^{2+} detection technology, yet current approaches are largely hampered by operational complexity and heavy-instrumentation dependence. The two most sensitive methods, fluorescence and electrochemical detections, rely on sophisticated, bulky and costly laboratory equipment that is not field-portable and requires controlled power supplies and operating environments. While colorimetric detection allows for naked-eye readout, its low sensitivity necessitates spectroscopic validation for quantitative analysis, which negates its portability advantage in most instances. Lab-scale detection also entails laborious sample pretreatment to mitigate matrix interference. Such processes are time-consuming and require specialized reagents and equipment, making them incompatible with rapid on-site screening. Consequently, raw sample analysis by unoptimized sensors leads to significant performance degradation due to the lack of necessary pretreatment resources in field settings. Additionally, practical operation poses notable barriers: electrochemical detection, in particular, requires trained personnel for precise electrode modification, calibration and operation, steps that are hard to implement in field settings with limited technical support, and even optical methods demand strict control of experimental parameters, a challenge without standardized, automated devices.

6.1.4 Scalability and cost limitations. Practical deployment of UO_2^{2+} detection technologies demands scalable synthesis and low production costs, yet most state-of-the-art sensing materials are fabricated *via* complex, low-yield lab-scale synthesis methods. These approaches are not suitable for

large-scale industrial production, leading to prohibitively high material costs that hinder widespread field application. Furthermore, poor reusability renders most sensors disposable, driving up long-term monitoring costs and generating chemical waste that poses an additional environmental burden at uranium-contaminated sites. Though some materials show regeneration potential, the associated processes typically require harsh chemical reagents and extra processing steps, making them unfeasible for on-site use.

In summary, the practical deployment of UO_2^{2+} detection technologies is constrained not merely by analytical performance, but by a combination of matrix interference, material instability, instrumentation and operational barriers, performance–practicality trade-offs and scalability issues. Addressing these challenges requires a paradigm shift from lab-scale optimization of detection limits and selectivity to design optimization for real-world applications. This entails integrating material engineering, matrix adaptation and device miniaturization to develop sensing systems that are stable, portable, low-cost and robust in complex environmental conditions, a critical focus for translating the remarkable advances in functional materials outlined in this review into actionable, field-deployable uranium monitoring technologies.

6.2 Future improvement directions

6.2.1 Enhancing selectivity for UO_2^{2+}. Achieving high selectivity in the presence of various interfering ions is critical for effective UO_2^{2+} detection. Functionalizing porous materials and nanomaterials with selective adsorbing groups, such as amidoxime, carboxyl, and phosphate groups, can enhance selectivity. Furthermore, tailoring the pore sizes of porous materials to fit the UO_2^{2+} ion can exploit the confinement effect, enhancing adsorption selectivity by limiting access to interfering ions. DNA-based materials, with their inherent ability for specific molecular recognition, can significantly improve selectivity through the incorporation of tailored nucleic acid sequences like DNAzymes, oligonucleotides, or aptamers.

6.2.2 Enhancing material stability. Improving the stability of detection materials in harsh environments (*e.g.*, extreme pH, seawater, or industrial waste) remains a critical challenge. Porous materials, such as MOFs and COFs, are often prone to hydrolysis and structural collapse under extreme conditions. To improve stability, materials can be designed with more robust chemical bonds or modified by introducing hydrophobic functional groups, such as fluorides, alkyl, or aromatic groups. Furthermore, combining porous materials with other materials, such as nanomaterials, hydrogels, or polymers, can enhance structural stability and introduce new functional properties that improve overall performance.

6.2.3 Improving sensitivity and accuracy. Detection in complex environmental samples often encounters interference from multiple factors, which can affect the accuracy and sensitivity of existing materials. One promising solution is multimodal detection, which combines various sensing techniques to provide complementary data, thus improving accuracy. For example, the oxidase-like activity of COFs under light can induce colorimetric changes, while the high conductivity of nanomaterials can enable electrochemical measurements. By combining these properties in a colorimetric-electrochemical dual-mode system, the detection sensitivity and reliability can be significantly improved. Additionally, integrating the inherent fluorescence of MOFs, the specific recognition capabilities of DNA-based materials, and the superparamagnetism of iron oxide nanoparticles into a unified multimodal system could lead to more reliable and accurate detection platforms.

6.2.4 Simplifying instrumentation and operations. To surmount instrumentation and operational hurdles for on-site UO_2^{2+} monitoring, future research should focus on device miniaturization, workflow simplification and pretreatment-free sensing system development, targeting portable, automated and field-adaptable detection without reliance on bulky lab equipment or professional technical support. For high-sensitivity fluorescence and electrochemical detection, microfabrication and microfluidic technologies will enable miniaturized, battery-powered portable detectors with integrated core modules for field use; colorimetric detection will be optimized *via* smartphone-assisted readout systems with custom optical accessories and image-analysis algorithms to achieve on-site quantitative analysis without spectroscopic validation. Operational workflows will be streamlined by developing prefabricated modified electrodes for electrochemical detection and standardized, automated all-in-one detection kits for all technologies, reducing professional operational demands and improving the reproducibility of on-site results. Pretreatment-free sensing systems, the key to resolving laborious on-site sample processing, will be engineered by endowing sensing materials with anti-interference, anti-fouling and *in situ* target enrichment properties, enabling direct, high-sensitivity UO_2^{2+} detection in raw complex samples without centrifugation, filtration and other pretreatment procedures.

6.2.5 Improving scalability and reducing costs. To tackle the scalability and cost limitations restricting widespread practical deployment of UO_2^{2+} detection technologies, future research should focus on developing scalable, low-cost material synthesis approaches and designing reusable sensing systems. Complex, low-yield lab-scale synthesis methods for advanced sensing materials need optimization for industrial scalability, with the adoption of simple, high-yield fabrication processes and low-cost raw materials to cut production costs and enable large-scale manufacturing. The reusability of sensors should be enhanced *via* rational material engineering to construct robust, anti-fouling structures, thereby reducing their replacement frequency and lowering long-term monitoring costs. For materials with regeneration potential, mild, on-site applicable regeneration protocols should replace harsh chemical-based processes, simplifying on-site reuse and eliminating chemical waste-related environmental burdens. The design of universal sensing platforms adaptable for UO_2^{2+} detection *via* simple modification can also further reduce costs, promoting the large-scale practical application of low-cost, reliable uranium detection technologies.

Looking ahead, future research on UO_2^{2+} detection should focus on the development of multifunctional composite

materials that integrate optical, electrochemical or multimodal sensing capabilities with enhanced selectivity, sensitivity and environmental stability. Such materials will address the core practical challenges, including complex matrix interference, poor material stability in harsh field settings, instrumentation and operational limitations, as well as scalability and cost constraints. Leveraging advances in computational chemistry and machine learning will yield valuable atomic-level insights into UO_2^{2+} recognition mechanisms and material degradation pathways, enabling the rational, predictive design of high-performance sensing materials, moving beyond empirical lab-scale optimization. More importantly, the seamless integration of such advanced materials with miniaturized, portable and field-adaptable detection devices, together with simplified, automated operational workflows and pretreatment-free sensing systems, will be pivotal to realizing real-time, on-site and reliable uranium contamination monitoring. Ultimately, the translation of these lab-scale innovations into efficient, cost-effective and robust UO_2^{2+} detection technologies will play a vital role in safeguarding the environment and human health, supporting the sustainable development of global nuclear energy and facilitating effective pollution control and environmental remediation at uranium-contaminated sites. By addressing the practical deployment challenges outlined in this review, we can advance uranium monitoring technologies that deliver long-term value for environmental protection and a more sustainable future.

Author contributions

KaiZeng Quan: writing – review & editing, writing – original draft, investigation. YuMin Wang: writing – review & editing, writing – original draft, investigation. Meng Qi: writing – original draft. Peng Xu: supervision, methodology. YaXing Wang: supervision, methodology. GuoXun Ji: writing – review & editing, investigation.

Conflicts of interest

There are no conflicts to declare.

Data availability

No primary research results, software or codes have been included, and no new data were generated or analysed as part of this review.

Acknowledgements

This work was supported by the National Natural Science Foundation of China (22476144).

Notes and references

1 L. Zhan, Y. Bo, T. Lin and Z. Fan, Development and outlook of advanced nuclear energy technology, *Energy Strategy Rev.*, 2021, **34**, 100630.
2 C. Degueldre, Uranium as a renewable for nuclear energy, Prog, *Nucl. Energy*, 2017, **94**, 174–186.
3 F. E. Arhouni, M. A. Saleh Abdo, S. Ouakkas, M. L. Bouhssa and A. Boukhair, Uranium recovery from Moroccan Phosphate rock for nuclear-powered desalination and water security: A review, *Radiat. Phys. Chem.*, 2025, **234**, 112802.
4 A. Durakovic, Medical effects of internal contamination with actinides: further controversy on depleted uranium and radioactive warfare, *Environ. Health Prev. Med.*, 2016, **21**, 111–117.
5 G. Steinhauser, A. Brandl and T. E. Johnson, Comparison of the Chernobyl and Fukushima nuclear accidents: A review of the environmental impacts, *Sci. Total Environ.*, 2014, **470–471**, 800–817.
6 S. Chandrakar, S. Sahu, S. Sharma and M. Pandey, A Review on the Efficiency of Adsorbents for Uranium Pollutant Remediation from Wastewater, *Trans. Indian Inst. Met.*, 2025, **78**, 55.
7 G. Bjørklund, Y. Semenova, L. Pivina, M. Dadar, M. M. Rahman, J. Aaseth and S. Chirumbolo, Uranium in drinking water: a public health threat, *Arch. Toxicol.*, 2020, **94**, 1551–1560.
8 E. Schnug and B. G. Lottermoser, Fertilizer-Derived Uranium and its Threat to Human Health, *Environ. Sci. Technol.*, 2013, **47**, 2433–2434.
9 A. K. Bairwa, K. Saini, S. K. Sahoo, S. N. Tiwari, T. Menaria and K. Gupta, Health risk study of groundwater uranium and terrestrial gamma radiation in Sawai Madhopur, Rajasthan (India), *J. Radioanal. Nucl. Chem.*, 2025, **334**, 6077–6089.
10 W. T. Yang, Q. H. Pan, S. Y. Song and H. J. Zhang, Metal-organic framework-based materials for the recovery of uranium from aqueous solutions, *Inorg. Chem. Front.*, 2019, **6**, 1924–1937.
11 W. W. He and D. B. Hua, Spectrographic sensors for uranyl detection in the environment, *Talanta*, 2019, **201**, 317–329.
12 P. Panwar, A. Joshi, K. P. Singh, M. Prasad, R. Mehra, S. K. Sahoo and R. C. Ramola, Distribution of uranium and selected toxic heavy metals in drinking water of Garhwal Himalaya, India, *J. Radioanal. Nucl. Chem.*, 2024, **333**, 2927–2935.
13 X. K. Shen and Y. F. Lu, Detection of uranium in solids by using laser-induced breakdown spectroscopy combined with laser-induced fluorescence, *Appl. Opt.*, 2008, **47**, 1810–1815.
14 M. Rezaee and F. Khalilian, Determination of uranium in water samples using homogeneous liquid-liquid microextraction via flotation assistance and inductively coupled plasma-optical emission spectrometry, *J. Radioanal. Nucl. Chem.*, 2015, **304**, 1193–1200.
15 H. Peng, H. Nan, S. Li, Y. Wang, Z. Dong, Z. Zhang, X. Cao and Y. Liu, Covalently construction of C-GSH-AuNCs@UiO-66-NH_2 composites as an efficient turn-on fluorescence sensor for UO_2^{2+}, *J. Solid State Chem.*, 2024, **334**, 124650.
16 Y. Zhan, X. Lu, T. Lan, Q. Tian, J. Shen and W. He, An AIE fluorescence sensor based on amidoxime for rapid

detection of uranyl ions in aqueous solutions, *Dyes Pigm.*, 2023, **216**, 111299.
17 S. J. Xiao, J. Huang, A. T. Qiu, G. Z. Liu, L. Zhang, T. Wu, Y. D. Shi and J.-D. Qiu, Advanced "turn-on" colorimetric uranium platform based on the enhanced nanozyme activity of a donor-acceptor structured covalent organic framework, *Anal. Chim. Acta*, 2024, **1302**, 342503.
18 X. Wu, Q. Huang, Y. Mao, X. Wang, Y. Wang, Q. Hu, H. Wang and X. Wang, Sensors for determination of uranium: A review, *TrAC, Trends Anal. Chem.*, 2019, **118**, 89–111.
19 K. Wu, Y. Zhou, Z. Zhou, X. Liang, J. Ma and L. Zhou, Electrochemical sensor modified with poly(toluidine blue) for monitoring trace uranium in natural water by stripping voltammetry, *J. Radioanal. Nucl. Chem.*, 2023, **332**, 3893–3901.
20 L. Zhang, M. Jia, X. Wang, L. Gao, B. Zhang, L. Wang, J. Kong and L. Li, A novel fluorescence sensor for uranyl ion detection based on a dansyl-modified peptide, *Spectrochim. Acta, Part A*, 2023, **292**, 122403.
21 S. H. Park, H. S. Kim and B. S. You, Improving the tensile strength of Mg-7Sn-1Al-1Zn alloy through artificial cooling during extrusion, *Mater. Sci. Eng., A*, 2015, **625**, 369–373.
22 X. Tang, H. Han, L. Li and H. Wang, Electrodes functionalized with advanced recognition materials for trace electrochemical sensing of uranyl ion, *Microchem. J.*, 2024, **199**, 109924.
23 J. Luo, X. Luo, Y. Gan, X. Xu, B. Xu, Z. Liu, C. Ding, Y. Cui and C. Sun, Advantages of Bimetallic Organic Frameworks in the Adsorption, Catalysis and Detection for Water Contaminants, *Nanomaterials*, 2023, **13**(15), 2194.
24 Q. Liu, Y. Yang, Y. Zou, L. Wang, Z. Li, M. Wang, L. Li, M. Tian, D. Wang and D. Gao, Fluorescent covalent organic frameworks for environmental pollutant detection sensors and enrichment sorbents: a mini-review, *Anal. Methods*, 2023, **15**, 5919–5946.
25 L. Farzin, M. Shamsipur, S. Sheibani, L. Samandari and Z. Hatami, A review on nanomaterial-based electrochemical, optical, photoacoustic and magnetoelastic methods for determination of uranyl cation, *Microchim. Acta*, 2019, **186**, 289.
26 L. Sun, J. Liu, L. Li, D. Zhen, Z. Dai, S. Tang, B. Zhu, L. Chen, H. Chen, M. Gong, Z. Tang and Y. Hu, Advances of biosensors for UO_2^{2+} detecting based on specific DNAzyme, *Inorg. Chem. Commun.*, 2022, **138**, 109234.
27 J. Perego, I. Villa, A. Pedrini, E. C. Padovani, R. Crapanzano, A. Vedda, C. Dujardin, C. X. Bezuidenhout, S. Bracco, P. E. Sozzani, A. Comotti, L. Gironi, M. Beretta, M. Salomoni, N. Kratochwil, S. Gundacker, E. Auffray, F. Meinardi and A. Monguzzi, Composite fast scintillators based on high-Z fluorescent metal-organic framework nanocrystals, *Nat. Photonics*, 2021, **15**, 393–400.
28 W. Cui, Y. Chen, W. Xu, K. Liu, W. Qiu, Y. Li and J. Qiu, A three-dimensional luminescent covalent organic framework for rapid, selective, and reversible uranium detection and extraction, *Sep. Purif. Technol.*, 2023, **306**, 122726.
29 Y. Bai, L. Xu, H. Chai, L. Zhou, G. Jiang and G. Zhang, Recent Advances on DNAzyme-Based Biosensors for Detection of Uranyl, *Front. Chem.*, 2022, **10**, 882250.
30 H. Liu, T. Fu and Y. Mao, Metal-Organic Framework-Based Materials for Adsorption and Detection of Uranium(VI) from Aqueous Solution, *ACS Omega*, 2022, **7**, 14430–14456.
31 N. Rani, P. Singh, S. Kumar, P. Kumar, V. Bhankar, N. Kamra and K. Kumar, Recent advancement in nanomaterials for the detection and removal of uranium: A review, *Environ. Res.*, 2023, **234**, 116536.
32 M. Sharma, P. Taneja, L. Yadav, P. Sharma, V. C. Janu and R. Gupta, Current insights into the implementation of electrochemical sensors for comprehensive detection and analysis of radionuclides, *Trends Anal. Chem.*, 2024, **178**, 117845.
33 J. Sun, D. Lin, Q. Wu, Z. Hong, X. Chen, Z. Liu, X. Liu, J. Cui, Z. Yuan and X. Xiao, Advances in CDs composites toward detection and adsorption of uranium and other radioactive elements: A review, *J. Environ. Chem. Eng.*, 2025, **13**, 118004.
34 C. Poulin-Ponnelle, D. Boudreau and D. Lariviere, Fluorescent Probes for Monitoring Toxic Elements from the Nuclear Industry: A Review, *Sensors*, 2025, **25**, 5835.
35 A. Amini, M. Khajeh, A. R. Oveisi, S. Daliran, M. Ghaffari-Moghaddam and H. S. Delarami, A porous multifunctional and magnetic layered graphene oxide/3D mesoporous MOF nanocomposite for rapid adsorption of uranium(VI) from aqueous solutions, *J. Ind. Eng. Chem.*, 2021, **93**, 322–332.
36 Y. Luo, N. Li, J. Tian, J. Pan, R. Su, V. Turkevich and L. Wang, Two birds with one stone strategy: selective uranium extraction and detection by a fluorescent covalent organic framework with high-affinity binding sites, *J. Mater. Chem. A*, 2025, **13**, 37458–37468.
37 S. Sauge-Merle, M. Recuerda, M. R. Beccia, D. Lemaire, R. Cherif, N. Bremond, F. Merola, Y. Bousmah and C. Berthomieu, Development of an Efficient FRET-Based Ratiometric Uranium Biosensor, *Biosensors*, 2023, **13**(5), 561.
38 S. Jampasa, W. Khamcharoen, S. Wirojsaengthong, A. Suea-Ngam, S. Traipop, T. Ozer, F. Unob, P. Puthongkham and O. Chailapakul, Recent advances and trends in the applications of nanomaterials in optical sensing platforms, *TrAC, Trends Anal. Chem.*, 2024, **180**, 117914.
39 X. Jiang, R. Yang, X. Lei, S. Xue, Z. Wang, J. Zhang, L. Yan, Z. Xu, Z. Chen, P. Zou and G. Wang, Design, Synthesis, Application and Research Progress of Fluorescent Probes, *J. Fluoresc.*, 2023, **34**, 965–975.
40 L. Jiao, J. Y. R. Seow, W. S. Skinner, Z. U. Wang and H.-L. Jiang, Metal-organic frameworks: Structures and functional applications, *Mater. Today*, 2019, **27**, 43–68.
41 L. Huang, Z. Liu and C. Tao, Strategies for constructing metal-organic frameworks-based biosensors and their applications in environmental pollutant detection, *J. Environ. Chem. Eng.*, 2025, **13**(3), 116806.

42 Q. Yu, M. Wang, X. Feng and X. Li, Research Progress of Rare Earth Metal-Organic Frameworks on Pollutant Monitoring, *Chemosensors*, 2025, **13**(5), 184.
43 M. D. Allendorf, C. A. Bauer, R. K. Bhakta and R. J. T. Houk, Luminescent metal-organic frameworks, *Chem. Soc. Rev.*, 2009, **38**, 1330–1352.
44 R. Huang, Z. Yu, Z. Li, X. Lin, J. Hou, Z. Hu and J. Zou, Photoluminescent metal-organic frameworks and their composites: Fundamentals, applications, and outlooks, *Coord. Chem. Rev.*, 2025, **526**, 216358.
45 X. Guo, L. Zhou, X. Liu, G. Tan, F. Yuan, A. Nezamzadeh-Ejhieh, N. Qi, J. Liu and Y. Peng, Fluorescence detection platform of metal-organic frameworks for biomarkers, *Colloids Surf., B*, 2023, **229**, 113455.
46 L. Feng, H. Wang, T. Feng, B. Yan, Q. Yu, J. Zhang, Z. Guo, Y. Yuan, C. Ma, T. Liu and N. Wang, In Situ Synthesis of Uranyl-Imprinted Nanocage for Selective Uranium Recovery from Seawater, *Angew. Chem., Int. Ed.*, 2022, **61**, 82–86.
47 H. Zhang, Y. Wang, W. Yan, J. Jin, Y. Wang, Y. Wang, J. Zhang, G. Wang, H. Dong and S. Zhang, Research progress of LMOFs containing aromatic carboxylic acid in anions recognition, *Microchem. J.*, 2024, **200**, 110453.
48 X. Li, H. Hao, L. Liu, H. Ren, J. Yin, J. Wang, L. Zhang, X. Zhang and L. Fan, Recent Advances in Metal-Organic Framework-Based Luminescent Sensors toward 3-Nitrotyrosine Biomarker, *Cryst. Growth Des.*, 2025, **25**, 7880–7902.
49 W. Hu, Y. Yang, S. Qie, Z. Mu, R. Xu, W. Li, Y. Chen, J. Qiao, L. Yue and M. Hu, The post-synthetic modification of a Cd-MOF and its fluorescence sensing properties, *Spectrochim. Acta, Part A*, 2026, **346**, 126867.
50 S. Jain, M. Nehra, R. Kumar, N. Dilbaghi, K. Kim and S. Kumar, Development of a FRET aptasensor based on MoS_2-doped Zn-MOF as luminophore for selective detection of cadmium in aqueous solutions, *Microchim. Acta*, 2024, **191**, 324.
51 L. Zhang, Y. He, Y. Wu, J. Zhang, S. Li and Z. Zhang, Highly sensitive ratiometric fluorescence detection of tetracycline residues in food samples based on Eu/Zr-MOF, *Food Chem.*, 2024, **436**, 137717.
52 X. Qin, W. Yang, Y. Yang, D. Gu, D. Guo and Q. Pan, A Zinc Metal–Organic Framework for Concurrent Adsorption and Detection of Uranium, *Inorg. Chem.*, 2020, **59**, 9857–9865.
53 L. Chen, D. Liu, J. Peng, Q. Du and H. He, Ratiometric fluorescence sensing of metal-organic frameworks: Tactics and perspectives, *Coord. Chem. Rev.*, 2020, **404**, 213113.
54 J. Zhang, Y. Ren, T. Xia, Y. Du, L. Shao, H. Tang and S. Yang, Post-synthesis metal-organic framework for turn-on ratiometric fluorescence sensing of UO_2^{2+}, *Z. Anorg. Allg. Chem.*, 2021, **648**, 41–46.
55 Y. Tong, L. Yu, X. Gong, L. Wu, Y. Chen, D. Wang, Y. Ye, F. Zhu, Z. Gong, J. Xu and G. Ouyang, On-Site Ratiometric Analysis of UO_2^{2+} with High Selectivity, *Anal. Chem.*, 2024, **96**, 3070–3076.
56 N. Huang, P. Wang and D. Jiang, Covalent organic frameworks: a materials platform for structural and functional designs, *Nat. Rev. Mater.*, 2016, **1**, 16068.
57 X. Li, S. Cai, B. Sun, C. Yang, J. Zhang and Y. Liu, Chemically Robust Covalent Organic Frameworks: Progress and Perspective, *Matter*, 2020, **3**, 1507–1540.
58 S. Raghav, J. Raghav, M. a. A. Muhammad, M. B. Singh, P. Jain and D. Kumar, Recent advancements in synthesis and applications of covalent organic frameworks, *Appl. Mater. Today*, 2025, **44**, 102694.
59 S. Liu, G. Liang, S. Wang and Q. Hu, Recent multifunctional applications of AIE-MOF/COF porous materials, *CrystEngComm*, 2025, **27**, 3643–3658.
60 L. Guo, L. Yang, M. Li, L. Kuang, Y. Song and L. Wang, Covalent organic frameworks for fluorescent sensing: Recent developments and future challenges, *Coord. Chem. Rev.*, 2021, **440**, 213957.
61 D. Zhen, C. Liu, Q. Deng, S. Zhang, N. Yuan, L. Li and Y. Liu, A review of covalent organic frameworks for metal ion fluorescence sensing, *Chin. Chem. Lett.*, 2024, **35**(8), 109249.
62 W. Cui, C. Zhang, W. Jiang, F. Li, R. Liang, J. Liu and J. Qiu, Regenerable and stable sp^2 carbon-conjugated covalent organic frameworks for selective detection and extraction of uranium, *Nat. Commun.*, 2020, **11**, 436.
63 D. Zhen, C. Liu, Q. Deng, L. Li, C. A. Grimes, S. Yang, Q. Cai and Y. Liu, Novel Olefin-Linked Covalent Organic Framework with Multifunctional Group Modification for the Fluorescence/Smartphone Detection of Uranyl Ion, *ACS Appl. Mater. Interfaces*, 2024, **16**, 27804–27812.
64 T. A. Saleh, Trends in nanomaterial types, synthesis methods, properties and uses: Toxicity, environmental concerns and economic viability, *Nano-Struct. Nano-Objects*, 2024, **37**, 101109.
65 Y. Pan, Z. Han, S. Chen, K. Wei and X. Wei, Metallic nanoclusters: From synthetic challenges to applications of their unique properties in food contamination detection, *Coord. Chem. Rev.*, 2023, **478**, 214964.
66 R. Jin and T. Higaki, Open questions on the transition between nanoscale and bulk properties of metals, *Commun. Chem.*, 2021, **4**, 28.
67 D. Feng, G. Zhang and Y. Li, Semiconductor Quantum Dots: Synthesis, Properties and Applications, *Nanomaterials*, 2024, **14**(22), 1825.
68 M. R. Kumalasari, R. Alfanaar and A. S. Andreani, Gold nanoparticles (AuNPs): A versatile material for biosensor application, *Talanta Open*, 2024, **9**, 100327.
69 H. Nan, Y. Liu, W. Gong, H. Peng, Y. Wang, Z. Zhang and X. Cao, An inner-filter-effect based ratiometric fluorescent sensor for the detection of uranyl ions in real samples, *Anal. Methods*, 2022, **14**, 532–540.
70 M. B. Cánchig, F. López, Z. Morales-Navarro, A. Debut, K. Vizuete, T. Terencio, M. Caetano and J. P. Saucedo-Vázquez, Enhanced selectivity of carbon quantum dots for metal ion detection through surface modification by heteroatom doping: A study on optical properties and theoretical approach, *Carbon Trends*, 2025, **18**, 100445.

71 Z. J. Zheng, L. Zhang, L. Z. Wang, Z. Q. Zhong, Y. T. Xiong, J. Guo, Z. B. Zhang, X. H. Cao and S. J. Xiao, Ultrasensitive detection of UO_2^{2+} based on dopamine-functionalized MoOx quantum dots, *Luminescence*, 2021, **37**, 127–133.

72 M. Hollenstein, DNA Catalysis: The Chemical Repertoire of DNAzymes, *Molecules*, 2015, **20**, 20777–20804.

73 B. Liu, G. Chen, A. M. Abd El-Aty, R. Zhai, G. Liu, X. Xu, Y. Zhang, L. Li, J. Zhang and D. Xu, Advances of functional nucleic acids based on specific recognition:A review, *Int. J. Biol. Macromol.*, 2025, **304**, 140828.

74 Z. Xiong, Q. Wang, J. Zhang, W. Yun, X. Wang, X. Ha and L. Yang, A simple and programmed DNA tweezer probes for one-step and amplified detection of UO_2^{2+}, *Spectrochim. Acta, Part A*, 2020, **229**, 118017.

75 J. Chen, X. Wang, J. Guo, Y. Lv, M. Chen, H. Tong and C. Liu, Heavy Metal-Induced Assembly of DNA Network Biosensor from Double-Loop Hairpin Probes for Ultrasensitive Detection of UO_2^{2+} in Water and Soil Samples, *Anal. Chem.*, 2024, **96**, 3153–3159.

76 F. Lin, Y. Cheng, M. Li, Z. Li and J. Dai, Detection of uranyl ions by single-hairpin based self-hybridization chain reaction, *Talanta*, 2025, **285**, 127374.

77 A. Kalintsev, A. Migdisov, J. Brugger and H. Xu, Uranium(VI) hydrolysis up to 250 °C and its geological implications, *Geochim. Cosmochim. Acta*, 2024, **377**, 68–83.

78 B. Pramanik, R. Sahoo and M. C. Das, pH-stable MOFs: Design principles and applications, *Coord. Chem. Rev.*, 2023, **493**, 215301.

79 R. Wei, X. Luo, G. Ning and D. Li, Covalent Metal-Organic Frameworks: Fusion of Covalent Organic Frameworks and Metal-Organic Frameworks, *Acc. Chem. Res.*, 2025, **58**, 746–761.

80 W. Liu, X. Dai, Z. Bai, Y. Wang, Z. Yang, L. Zhang, L. Xu, L. Chen, Y. Li, D. Gui, J. Diwu, J. Wang, R. Zhou, Z. Chai and S. Wang, Highly Sensitive and Selective Uranium Detection in Natural Water Systems Using a Luminescent Mesoporous Metal-Organic Framework Equipped with Abundant Lewis Basic Sites: A Combined Batch, X-ray Absorption Spectroscopy, and First Principles Simulation Investigation, *Environ. Sci. Technol.*, 2017, **51**, 3911–3921.

81 N. Seal, A. Karmakar, S. Kundu and S. Neogi, Pendent carboxylic acid-fuelled high-performance uranium extraction in a hydrogen-bonded framework and prolifically improved water oxidation via post-metalation-actuated composite fabrication, *J. Mater. Chem. A*, 2024, **12**, 3501–3512.

82 V. Venkata Sravani, S. Tripathi, B. Sreenivasulu, S. Kumar, S. Maji, C. V. S. Brahmmananda Rao, A. Suresh and N. Sivaraman, Post synthetically modified IRMOF-3 for efficient recovery and selective sensing of U(vi) from aqueous medium, *RSC Adv.*, 2021, **11**, 28126–28137.

83 C. Zhang, W. Cui, W. Jiang, F. Li, Y. Wu, R. Liang and J. Qiu, Simultaneous sensitive detection and rapid adsorption of UO_2^{2+} based on a post-modified sp2 carbon-conjugated covalent organic framework, *Environ. Sci.: Nano*, 2020, **7**, 842–850.

84 W. Cui, W. Xu and W. Qiu, Constructing an ultrastable imidazole covalent organic framework for concurrent uranium detection and recovery, *Ecotoxicol. Environ. Saf.*, 2023, **252**, 114639.

85 Q. Wang, T. Han, C. Miao, W. Qin and X. Wu, A fluorescent N-doped carbon dot-hydrogel composite for concurrent selective detection and local hot spot promoted adsorption of uranium(vi), *Environ. Sci.:Water Res. Technol.*, 2023, **9**, 2680–2691.

86 R. Lu, Y. Luo, L. Su, S. Ye, X. Wang, W. Ren, J. Zhang, F. Zhao and C. Zheng, Field Detection of Uranyl in Coastal Water of China Using a Portable Device via DNA Photocleavage, *Anal. Chem.*, 2024, **96**, 11525–11532.

87 X. Zhang, Y. Wang, M. Gong, L. Xiong, J. Song, S. Chen, Y. Tong, Y. Liu, L. Li and D. Zhen, Engineering an upconversion fluorescence sensing platform with "off-on" pattern through specific DNAzyme-mediated signal amplification for supersensitive detection of uranyl ion, *Microchim. Acta*, 2024, **191**, 503.

88 I. Ahmad, T. Muhmood, A. Rehman, M. Zahid, M. Abohashrh, S. Nishat, Y. Raharjo, Z. Zhou and X. Yang, Zeolite imidazole framework entrapped quantum dots (QDs@ZIF-8): encapsulation, properties, and applications, *J. Taiwan Inst. Chem. Eng.*, 2023, **149**, 104993.

89 A. Cui, X. Wu, J. Ye, G. Song, D. Chen, J. Xu, Y. Liu, J. Lai and H. Sun, "Two-in-one" dual-function luminescent MOF hydrogel for onsite ultra-sensitive detection and efficient enrichment of radioactive uranium in water, *J. Hazard. Mater.*, 2023, **448**, 130864.

90 X. Mao, Y. Cai, Q. Luo, X. Liu, Q. Jiang, C. Zhang, L. Zhang, R. Liang and J. Qiu, Europium(III) Functionalized Covalent Organic Framework as Sensitive and Selective Fluorescent Switch for Detection of Uranium, *Anal. Chem.*, 2024, **96**, 5037–5045.

91 S. Yang, W. Li, Z. Li, X. Zeng, Q. Wang, C. Yan, L. Pan, Y. Chen, M. Mu, C. Li and W. Yang, Water-soluble, SDS-functionalized CdSe/CdS/ZnS quantum dots for uranium detection in aqueous environments, *Ceram. Int.*, 2024, **50**, 23493–23499.

92 F. Yang and L. Ge, Colorimetric Sensors: Methods and Applications, *Sensors*, 2023, **23**(24), 9887.

93 S. Lee, H. Yoo and J. Y. Kim, Recent advances on MOF-based colorimetric sensors, *Bull. Korean Chem. Soc.*, 2025, **46**, 918–939.

94 Z. Zhou, W. He, H. Chao, H. Wang, P. Su, J. Song and Y. Yang, Insertion of Hemin into Metal-Organic Frameworks: Mimicking Natural Peroxidase Microenvironment for the Rapid Ultrasensitive Detection of Uranium, *Anal. Chem.*, 2022, **94**, 6833–6841.

95 Y. Feng, Y. Xu, S. Liu, D. Wu, Z. Su, G. Chen, J. Liu and G. Li, Recent advances in enzyme immobilization based on novel porous framework materials and its applications in biosensing, *Coord. Chem. Rev.*, 2022, **459**, 214414.

96 Y. Xu, J. Wei and X. Chen, Visible Light-Responsive Sulfone-Based Covalent Organic Framework as Metal-Free Nanoenzyme for Visual Colorimetric Determination of Uranium, *Chemosensors*, 2022, **10**(7), 248.

97 S. Sangwan and R. Seth, Synthesis, Characterization and Stability of Gold Nanoparticles (AuNPs) in Different Buffer Systems, *J. Cluster Sci.*, 2021, **33**, 749–764.
98 L. Zhang, D. Huang, P. Zhao, G. Yue, L. Yang and W. Dan, Colorimetric detection for uranyl ions in water using vinylphosphonic acid functionalized gold nanoparticles based on smartphone, *Spectrochim. Acta, Part A*, 2022, **269**, 120748.
99 L. Zhang, S. Shi, P. Xiong, L. Chen, J. Xu, J. Jiang, S. Yang and H. Wu, DNAzyme recognition triggered cascade signal amplification for rapid and highly sensitive visual detection of uranyl ions, *Analyst*, 2022, **147**, 4158–4166.
100 Y. Lei, Y. Li, C. Liu, L. He, Q. Li, L. Liao and X. Xiao, Smartphone-assisted colorimetric determination of uranyl ions in aqueous solutions, *New J. Chem.*, 2023, **47**, 4667–4673.
101 S. A. Hashemi, A. Ghaffarkhah, A. A. Isari, M. Panahi-Sarmad, F. Jiang, O. J. Rojas, S. Wuttke, M. Dincă and M. Arjmand, Advancing from MOFs and COFs to Functional Macroscopic Porous Constructs, *Adv. Mater.*, 2025, **37**, 2411617.
102 J. Song, L. Chai, M. Zhao, Y. Sun, X. Li and J. Pan, J. Research progress on metal organic framework derived porous carbon though interfacial engineering and synergistic effect, *Power Sources*, 2024, **604**, 234471.
103 X. Cao, Y. Sun, Y. Wang, Z. Zhang, Y. Dai, Y. Liu, Y. Wang and Y. Liu, PtRu bimetallic nanoparticles embedded in MOF-derived porous carbons for efficiently electrochemical sensing of uranium, *J. Solid State Electrochem.*, 2020, **25**, 425–433.
104 B. Sun and L. Cui, Rational Design of Covalent Organic Frameworks for Enhanced Reticular Electrochemiluminescence and Biosensing Applications, *Biosensors*, 2025, **15**(11), 760.
105 W. Cui, Y. Li, Q. Jiang, Q. Wu, Q. Luo, L. Zhang, R. Liang and J. Qiu, Covalent Organic Frameworks as Advanced Uranyl Electrochemiluminescence Monitoring Platforms, *Anal. Chem.*, 2021, **93**, 16149–16157.
106 E. Kianfar and H. Sayadi, Recent advances in properties and applications of nanoporous materials and porous carbons, *Carbon Lett.*, 2022, **32**, 1645–1669.
107 J. Han, J. Gao, J. Chen, G. Qi, Y. Gui, Y. Wang, Y. Yan, F. Ma, Q. Chen and Y. Xue, Electrochemical measurements of uranyl ions in real nuclear wastewater using nanogold-modified electrodes, *Microchem. J.*, 2025, **212**, 113340.
108 J. Wang, H. Zhou, J. Liu, J. He, J. Liu and W. Yang, Electrochemical detection of DNA by formation of efficient electron transfer pathways through adsorbing gold nanoparticles to DNA modified electrodes, *Microchem. J.*, 2021, **169**, 106581.
109 S. Guo, J. Lin, L. Lin, W. Xu, Y. Guo, Z. Xu, C. Lu, X. Shi, L. Chen and H. Yang, Selecting small molecule DNA aptamers with significant conformational changes for constructing transcriptional switches and biosensors, *Sci. China:Chem.*, 2023, **66**, 1529–1536.
110 S. E. Jett and A. J. Bonham, Reusable Electrochemical DNA Biosensor for the Detection of Waterborne Uranium, *ChemElectroChem*, 2017, **4**, 843–845.
111 Z. Chen, J. Liu, W. Wang, G. Qin, S. Liu, W. Zhang, C. Peng, Y. Tan, Z. Dai, D. Zhen and L. Li, Aptamer-regulated colorimetric and electrochemical dual-mode sensor for the detection of uranyl ions utilizing AuNCs@COF composite, *Microchim. Acta*, 2025, **192**, 295.
112 S. Shi, H. Wu, L. Zhang, S. Wang, P. Xiong, Z. Qin, M. Chu and J. Liao, Gold nanoparticles based electrochemical sensor for sensitive detection of uranyl in natural water, *J. Electroanal. Chem.*, 2021, **880**, 114884.
113 Z. Wang, H. Gao, P. Liu, X. Wu, Q. Li, J. Xu and D. Hua, Visualized uranium rapid monitoring system based on self-enhanced electrochemiluminescence-imaging of amidoxime functionalized polymer nanoparticles, *Chin. Chem. Lett.*, 2022, **33**, 3456–3460.
114 M. Xiang, C. Yin, Q. Chen, G. Zhu, Z. Chen, H. Li, R. Antwi-Baah, J. Tang, K. Yang and S. Xu, A label-free electrochemical biosensor for detection of uranyl ions in water based on nucleic acid dye-inducing turn-off of photosensitization, *Microchem. J.*, 2025, **213**, 113811.
115 C. Jiang, X. Tang, B. He, Y. Ouyang, R. Xiang and L. Li, Amidoxime-grafted fluorinated graphene nanosheets as a trace electrochemical sensing platform of uranyl ion, *Microchem. J.*, 2024, **205**, 111371.
116 L. Chen, J. Liu, C. Cao, S. Tang, C. Lv, X. Xiao, S. Yang, L. Liu, L. Sun, B. Zhu and L. Li, Dual-signal amplification electrochemical sensing for the sensitive detection of uranyl ion based on gold nanoparticles and hybridization chain reaction-assisted synthesis of silver nanoclusters, *Anal. Chim. Acta*, 2021, **1184**, 338986.
117 L. Xiong, Y. Tong, J. Song, S. Chen, Y. Liu, J. Liu, L. Li and D. Zhen, Smartphone-assisted fluorescence/colorimetric dual-mode sensing strategy for uranium ion detection using cerium-sulfonyl calix[4]arene, *Microchim. Acta*, 2025, **192**, 158.
118 Y. Wu, X. Tan, H. Gong, M. Wang, G.-l. Wu, N. Li, F. Liu, H. Xia, L. Tang and Q. Yang, Self-assembled TMB-CuO_2 nanosheets for dual-mode colorimetric and NIR-II photothermal detection of uranyl ion, *Anal. Chim. Acta*, 2025, **1356**, 344041.